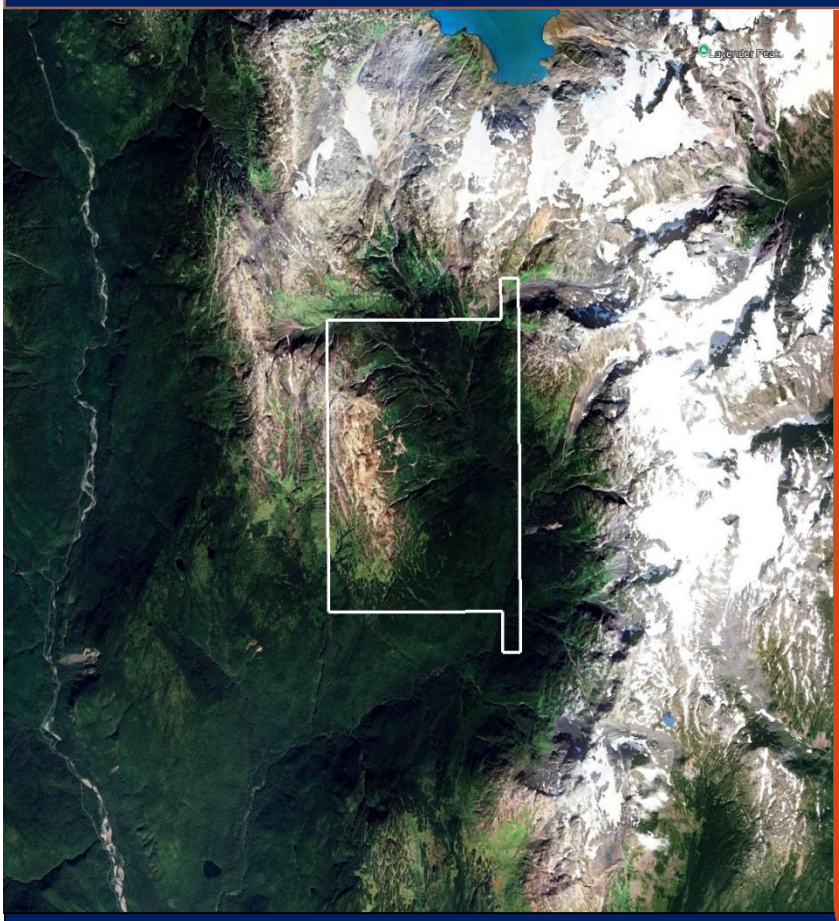
Data Acquisition and Processing Report

Helicopter-borne **MobileMT**

Electromagnetic & Magnetic survey





Ajax MobileMT Project

in Stewart, BC

for Korestar Exploration Inc.,

by Expert Geophysics Surveys Inc.

Address:

1145 Nicholson Rd, Unit 1, Newmarket ON, L3Y 9C3;

Tel: (+1) 382-398-4723 (EGS)

info@expertgeophysics.com

www.expertgeophysics.com

'Expert Geophysics' Job 26132

October 2026

Contents

1 Executive Summary 3
2 Introduction 4
3 Survey Areas and Flight Specifications 6
3.1 Ajax Block 7
4 Field Operations 8
4.1 Operations Schedule 8
4.2 Aircraft Parking and Base Station Locations 8
4.3 Re-flights 8
4.4 Office and Field Personnel 9
5 Survey Equipment and Specifications 10
5.1 Equipment Composition 10
5.2 The Airborne Magnetometer System 12
5.3 The Airborne GPS Navigation System 12
5.4 Data Acquisition System 13
5.5 Radar-Altimeter 13
5.6 MobileMT Ground Base Station 13
5.7 MobileMT Magnetometer Base Station 13
5.8 Field Computer Workstation 14
6 Data Processing and Deliverables Specifications 15
6.1 MobileMT EM Data Processing 15
6.2 MobileMT Apparent Conductivity Axes Anomalies Tracing 15
6.3 MobileMT EM Data Inversions 16
6.4 Magnetic Data Processing 18
6.5 Magnetic Field Data Inversions 19
6.6 VLF Data Processing 19
6.7 Ancillary Data Processing 20
6.8 Data Deliverables 20
7 Survey Results General Analysis and Recommendations 25
8 Conclusions and Recommendations 35
9 References 37
Appendix I Company Profile 39
Appendix II MobileMT Electromagnetic Technology 40
Appendix III MobileMT Maps Images 44

Tables

Table 1 – Summary Project Information 5
Table 2 – Coordinates of the Ajax block boundary (WGS 84, UTM zone 9N) 7
Table 3 – Flight lines specifications for Ajax 7
Table 4 – Operations schedule 8
Table 5 – Aircraft parking and base station locations 8
Table 6 – List of re-flown lines 8
Table 7 – Frequency gates extracted from the data (Hz) for the Ajax Block. 11
Table 8 – Geosoft 26132_Ajax_EM.gdb Data Format 20
Table 9 – Geosoft 26132_Ajax_Mag.gdb Database Format 21
Table 10 – Geosoft 26132_Ajax_VLF.gdb Database Format 22
Table 11 – List of Ajax Block grids (in Geosoft format) and maps (in Geosoft and PDF formats). 22

Figures

Figure 1 – Ajax Survey Area Location. 6
Figure 2 – Ajax block flight path 7
Figure 3 - MobileMT system tow-bird on flight 10
Figure 4 – EGL Navigation Computer, Moving-map Display 12
Figure 5 – Pilot Steering Indicator and Radio Altimeter Indicator 12
Figure 6 – Example of tracing axes of apparent conductivity anomalies in profile and plan view. 16
Figure 7 – Example of unstructured model mesh used as input to 2D inversions along a line segment of the survey. 17
Figure 8 – Agreement between observed (points) and modelled (lines) apparent resistivity profiles along a line segment of the survey. 18
Figure 9 – Agreement between observed (points) and modelled (lines) apparent resistivity curves for stations along a line segment of the survey. 18
Figure 10 – Data types loaded into 26132_Ajax_GA Project.geoh5 Geoscience Analyst Workspace. 23
Figure 11 – Example of data visualization options in Geoscience Analyst (top: plan map of TMI grid; Bottom: Voxel slices and section image) 24
Figure 12 – left: Regional geologic map of the northwestern Stikinia Terrane with Cu(±Au±Mo) porphyry (yellow) and vein and breccia-hosted (including epithermal) deposits (red; Colpron and Nelson, 2011) and right: a close-up simplified geologic map of the Ajax MobileMT survey block (outlined in red) with locations of nearby deposits (modified after Miller et al., 2020) 26
Figure 13 – Geologic map of the survey area with the Ajax MobileMT survey lines. 26
Figure 14 – Resistivity voxel in 3D view. Top: at surface, bottom: at 400 m ASL. 29
Figure 15 – Apparent conductivity (133 Hz) color grid with overlapped contours total magnetic intensity anomalies. 30
Figure 16 – Apparent conductivity anomalies axes from 106-212 Hz data over total magnetic intensity 31
Figure 17 – Magnetic Susceptibility (top) and Resistivity (bottom) sections along L1032 (location shown in Figure 15). Sections shown from W → E. Locations of drillholes are marked. 32
Figure 18 – Magnetic Susceptibility (top) and Resistivity (bottom) sections along L1060 (location shown in Figure 15). Sections shown from W → E. Locations of drillholes are marked. 33
Figure 19 – Magnetic Susceptibility (top) and Resistivity (bottom) sections along L1092 (location shown in Figure 15). Sections shown from W → E. Locations of drillholes are marked. 34

1 Executive Summary

Expert Geophysics Surveys Inc. (EGS) conducted a helicopter-borne **MobileMT** electromagnetic and magnetic survey in Stewart, BC for **Korestar Exploration Inc**. Electromagnetic and magnetic geophysical data were acquired using Expert Geophysics Limited's (EGL) airborne **MobileMT** system. Please refer to Appendix I for the Company Profile and Appendix II for a description of the **MobileMT** technology.

The purpose of the survey was mapping bedrock structure and lithology, including possible alteration and mineralization zones, observing apparent conductivity corresponding to different frequencies, inverting EM data to obtain the distribution of resistivity with depth, and using VLF and magnetic data to study properties of the bedrock units. A total of 2 production flights were flown to complete 230 line-kilometers of the survey over a 19 sq.km area.

The survey was flown using an AS350SB2 helicopter, registration C-FTSB, of the aviation company Interior Helicopters. The survey production flights started on 11-August-2026 and data acquisition was completed on 12-August-2026. The survey operations were conducted from Stewart, BC.

The survey lines are oriented N-S (N 0° E) at 100 m spacing, while tie lines are oriented perpendicular to the survey lines and spaced at 1000 m.

The geophysical survey results are presented in the form of digital databases, maps, grids, sections, elevation slices and 3D voxels. The report describes the data acquisition, processing and inversion procedures, equipment and digital data specifications, and basic data analysis.

2 Introduction

This report describes the **MobileMT** airborne electromagnetic and magnetic survey **Expert Geophysics Surveys Inc.** (**EGS**, Appendix I) performed for **Korestar Exploration Inc.** during the period of August 11 to 12, 2026, over a survey block located in Stewart, BC. Electromagnetic passive fields and magnetic field data were gathered using the **MobileMT** helicopter-borne system (Appendix II).

The Survey Area section of the report contains a description of the survey area and flight paths. The Field Operations section includes information about the operation flow, the airport and base station locations and flights dates. The Survey Equipment section describes the main and ancillary equipment used for data acquisition. The Data Processing and Deliverables Specifications section consists of main data processing and inversion procedures and final products description. The Survey results discussion section includes basic data analysis and recommendations for further data analysis.

The following table includes a brief reference of the survey specifications (Table 1).

Table 1 – Summary Project Information

Client:	**Korestar Exploration Inc.**
Client contact:	Ian Webster Email: ianwebster@telus.net
EGS Job Number	26132
Survey area location:	Stewart, BC
Crew and aircraft location:	Stewart, BC
Mag Base station location:	WGS 84 UTM zone 9N 475478 m E, 6163408 m N
EM Ref station location:	WGS 84 UTM zone 9N 475525 m E, 6163372 m N
Block:	Ajax
Total line kms:	230 line-km
Total Survey Area:	19 sq.km
Traverse line direction/spacing:	0°; 100 m
Tie lines direction/spacing:	90°; 1000 m
Dates flown:	August 11 to 12, 2026
Helicopter:	AS350SB2, C-FTSB, Interior Helicopters
Average survey speed:	18 m/sec
Average Helicopter terr. clearance:	191 m
Average magnetometer clearance:	123 m
Average EM sensor clearance:	103 m
Coordinates Datum:	WGS 84
Coordinates Projection:	UTM zone 9N, Central Meridian 129° W (Zone 9N)
MobileMT extracted frequencies Hz:	33, 42, 51, 68, 84, 106, 133, 167, 212, 266, 338, 424, 534, 673, 4274, 5384, 6785, 8550, 10772, 13572
VLF extracted frequencies, kHz:	19.80, 24.00, 24.80

3 Survey Areas and Flight Specifications

The **MobileMT** Ajax Block survey area is located near Stewart, BC (Figure 1).

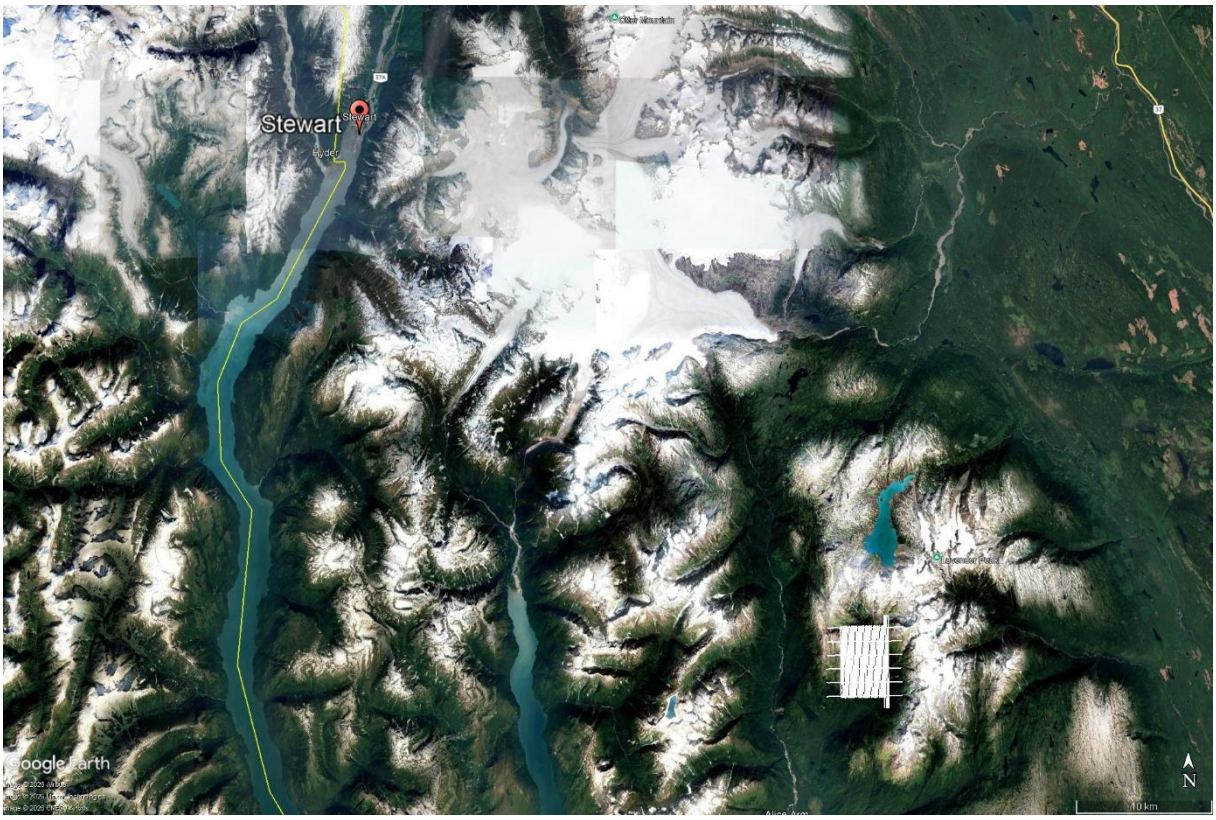


Figure 1 – Ajax Survey Area Location.

The survey was flown with an AS350SB2 helicopter, registration C-FTSB, operated by the Interior Helicopters aviation company.

- Average terrain clearance of the helicopter during the survey was 191 m, at average speeds of 18 m/sec.
- Average terrain clearance of the magnetometer bird during the survey was 123 m.
- Average electromagnetic sensor terrain clearance 103 m.

3.1 Ajax Block

The **MobileMT** Ajax Block is located about 50 km SE from Stewart, BC (Figure 1). Flight paths over the survey blocks are presented in Figure 2.

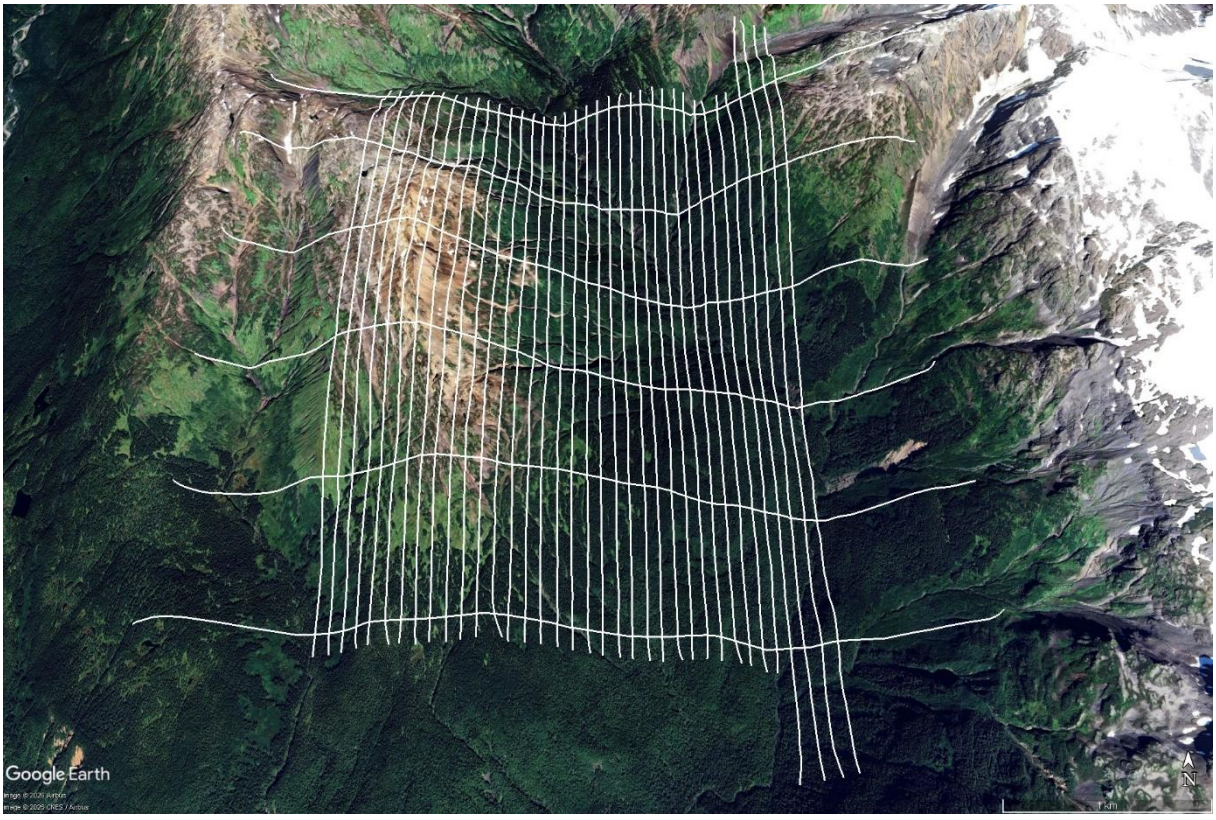


Figure 2 – Ajax block flight path

The "WGS 84 /UTM zone 9N" coordinate system information is displayed in Table 2. The survey flight lines specifications are in Table 3.

Table 2 – Coordinates of the Ajax block boundary (WGS 84, UTM zone 9N)

Block Boundary					
X	Y	X	Y	X	Y
473138	6162413	476638	6163162	476313	6157088
476313	6162413	476638	6156338	473138	6157088
476313	6163162	476317	6156337		

Table 3 – Flight lines specifications for Ajax

Line spacing, m	Lines direction	Line numbers	# of lines	Line kms
100 m (traverse)	0°	L1000-L1350	36	197
1000 m (tie)	90°	T8000-T8050	6	33
		Total	**42**	**230**

4 Field Operations

4.1 Operations Schedule

The survey operations were conducted from Stewart, BC. The survey was executed in 2 production flights starting on 11-August-2026 and data acquisition was completed on 12-August-2026. A description of the daily survey activities is provided in Table 4.

Table 4 – Operations schedule

Date	Flight No	estim. flown, km	Operation
2026-08-08			System Assembly
2026-08-09			Testing
2026-08-10			Standby
2026-08-11	F24001	120.97	Production flight was completed
2026-08-12	F24002	95.03	Production flight was completed

4.2 Aircraft Parking and Base Station Locations

Locations of the aircraft parking, magnetic base station and MobileMT reference base station are specified in Table 5.

Table 5 – Aircraft parking and base station locations

	Position
Aircraft parking	Stewart, BC
Mag base station	WGS 84 UTM zone 9N 475478 m E, 6163408 m N
EM Ref station	WGS 84 UTM zone 9N 475525 m E, 6163372 m N

4.3 Re-flights

Identified, during the survey quality control (QC), and re-flown flight-lines for the Ajax Block are specified in Table 6. Only accepted by QC lines data are included into the final databases.

Table 6 – List of re-flown lines

Line Number	Length, km	Reason
None	None	None

4.4 Office and Field Personnel

The following personnel participated in the project support and field operations:

Project Managers:	Andrei Bagrianski, PhD, P.Geo
	Werner Hilla
	Alejandro Heredia
	Hector Martinez
EGS Operator/Crew chief:	Matt Lyon
EGS Operator:	Patricio Alcayaga
DataQC, Processor:	Julian Boada, B.Sc. Honours under the management of
	Andrei Bagrianski, PhD, P.Geo and Sina Kamyab, MSc
Technical support:	under the management of Mikhail Kuzmin, MSc.
Pilots:	Jordan Luck (Interior Helicopters)
Final data processing, finals, report:	Alexander Prikhodko, PhD, P.Geo
	Emily Data, BSc Honours. P.Geo
	Aamna Sirohey, MSc, P.Geo
	Zihao Han, PhD., P.Geo
	Patrick Yee, BSc
	Janine Dela Cruz, BSc, G.I.T
	Robiah Al Wardah, PhD

5 Survey Equipment and Specifications

5.1 Equipment Composition

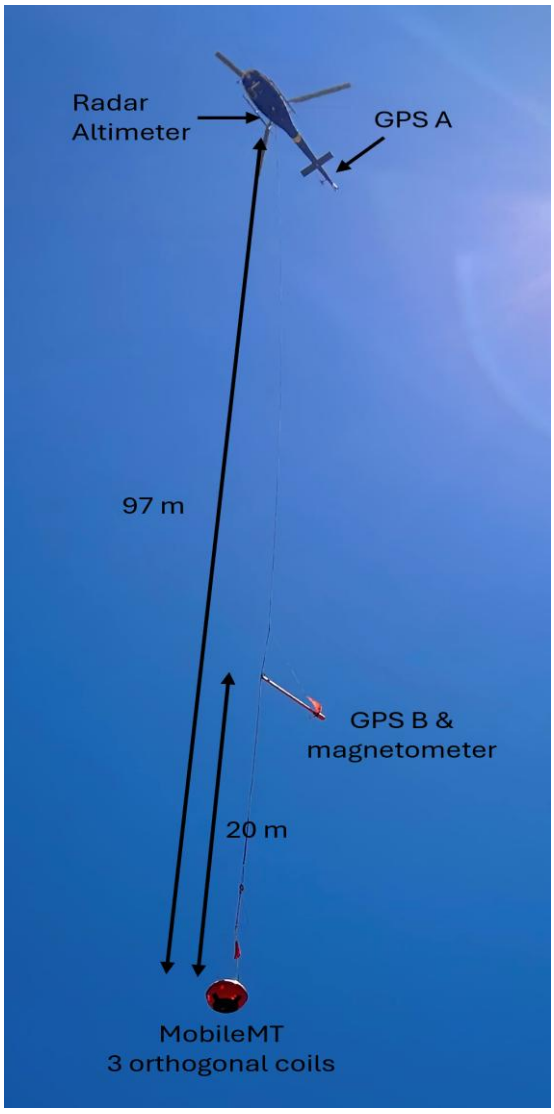


Figure 3 - MobileMT system tow-bird on flight

The main instrumentation installed on the **MobileMT** tow-bird (Figure 3):

- Three orthogonal induction coils to measure naturally occurring magnetic fields in the frequency range 25 Hz – 20,000 Hz
- Geometrics G822A Cesium Magnetometer, installed in a separate towed-bird, 20 m above the **MobileMT** bird, sensitivity of 0.001 nT/10 Hz sampling
- GPS antenna, installed on the towed-bird with the magnetometer.

The main instrumentation installed on the helicopter:

- EGL PC-104 based Data Acquisition System
- EGL Navigation system with Pilot Steering Indicator
- Smartmicro model UMRR-0A Radio Altimeter, 0 – 500 m range
- GPS antenna, installed on the helicopter tail

Base Stations and Ground Support instrumentation comprises:

- **MobileMT** Ground Base Station, 4-channel (2 channels for signal and 2 channels for reference signal), to measure variations of the electric field in two directions with 4 pairs of electrodes. Electrical line length –50m each line, direction YX – 182°, YZ – 115°
- GEM Systems GSM-19 Base Station Magnetometer, 0.1 nT sensitivity, with data logger;
- A Field Data Processing Workstation and a full suite of software for the quality control and preliminary processing of the airborne geophysical data.

MobileMT VLF specifications:

- VLF System: EGL proprietary digital system
- Model: Matrix Plus
- Manufacturer: EGL
- Antenna: used in the MobileMT three orthogonal coils (x,y,z)
- Primary Sources: up to 8 discrete frequencies (stations)
- Output Parameters: Amplitude (total field)
- Sample Rate: 0.1 second

- Gain: Constant gain setting
- Filtering: No filtering

MobileMT EM specifications:

- Airborne receiver: Three orthogonal induction coils (1.4 m diameter each)
- Airborne shell: Aerodynamic shaped capsule
- Digitizing rate: 73,728 Hz
- Tow cable length: 97 m
- Ground sensors 4 pairs of electrodes
- Electrode separation 50 m
- EM base station line directions 182 °, 115 °
- Frequency range: 25 Hz – 20,000 Hz
- Output computed parameters: Apparent conductivity for selected frequencies
- Output frequencies: Selectable from 25 Hz – 20,000 Hz depending on signal strength.

Selected frequencies and corresponding frequency gates are in Table 7

Table 7 – Frequency gates extracted from the data (Hz) for the Ajax Block.

Start	End	Center
28.7	38.4	33.0
36.1	48.3	42.0
45.5	60.9	51.0
57.3	76.7	68.2
72.3	96.6	84.0
91.0	121.8	105.9
114.7	153.4	133.4
144.5	193.3	167.3
182.1	243.5	211.9
229.4	306.8	266.0
289.0	386.6	338.2
364.1	487.1	424.4
458.8	613.7	534.1
578.0	773.2	673.4
3670.3	4909.3	4273.7
4624.3	6185.3	5384.0
5826.2	7793.0	6784.9
7340.6	9818.5	8549.8
9248.6	12370.6	10772.1
11652.5	15585.9	13571.7

5.2 The Airborne Magnetometer System

The airborne magnetometer is a state-of-the-art system developed by EGL. It utilizes a Geometrics G822A cesium magnetometer sensor, installed in the towed-bird with a high accuracy Larmor frequency counter.

5.3 The Airborne GPS Navigation System

EGL uses a proprietary GNSS receiver system utilizing RXM-GNSS-TM GPS Engines. The key features of the receiver are:

- L1 1575.42MHz, C/A code
- 33-channel satellite tracking
- Position accuracy: 2.5m
- 10 Hz update rate
- Constellation System Support:
  - GPS
  - GLONASS
  - GALILEO
  - QZSS
- DGPS support:
  - (SBAS) Satellite-Based Augmentation System
  - (RTCM) Radio Technical Commission for Maritime Services
  - (WAAS) Wide-Area Augmentation System
  - (EGNOS) European Geo-Stationary Navigation System
  - (MSAS) MTSAT Satellite-Based Augmentation System
  - (GAGAN) GPS-Aided Geo-Augmented Navigation

An EGL Computer/Pilot Steering Indicator is used to compute the flight path grids in real-time onboard the helicopter (Figure 4, Figure 5).



Figure 4 – EGL Navigation Computer, Moving-map Display



Figure 5 – Pilot Steering Indicator and Radio Altimeter Indicator

5.4 Data Acquisition System

The data acquisition system features an EGL PC-104-based data acquisition system. The EGL data acquisition system is an instrument developed by EGL for airborne geophysical data acquisition tasks. It features EGL proprietary technology and software. The EGL data acquisition system simultaneously records data on internal flash disk and displays it on a color LCD display, at a repetition rate of 0.33 sec, for post-flight computer processing. The five main functions fulfilled by the data acquisition system are: 1) system control and monitoring, 2) data acquisition, 3) real-time data processing, 4) navigation, and 5) data playback and analysis.

5.5 Radar-Altimeter

A Smartmicro model UMRR-0A radar altimeter system records the ground clearance to an accuracy of 3% over a range of 0 ft to 1,640 ft (0 to 500 m). The altimeter is interfaced to the navigation system and the data acquisition system with an output repetition rate of 10 Hz and digitally recorded.

5.6 MobileMT Ground Base Station

The MMT Ground Base Station comprises:

- 4 pairs of electrodes, 50 m separation each;
- Line directions 182 °, 115 °;
- EGL PC-104 based Data Acquisition System with a GPS system to record the GPS time together with the electric data;
- A power supply unit.

5.7 MobileMT Magnetometer Base Station

The Magnetometer Base Station was a GSM-19 Overhauser magnetometer. The base-station magnetometer, with digital recording, operated continuously throughout the airborne data acquisition, with a sampling interval of 1 seconds, and sensitivity of 0.1 nT. The ground and airborne system clocks synchronized using GPS time, to an accuracy of far better than 1 second. At the end of the day's work, the digital data transferred from the base station's data-logger to the FWS. This base station is located in a place with low magnetic gradient (less than 2nT/m). The base station sited away from moving steel objects, vehicles or hydro transmission lines to ensure minimum interference and noise levels.

5.8 Field Computer Workstation

The Field Data Processing Workstation (FWS) is a dedicated computer system for use at the technical base in the field. The workstation to be used on this project is designed for use with Geosoft OASIS Data Processing Software. It is also capable of processing and imaging all the geophysical and navigation data acquired during the survey, producing semi-final, preliminary-levelled maps.

The main features of the FWS are:

- Portability;
- Digital Data Verification - flight data quality and completeness were assured by both statistical and graphical means;
- Flight Path Plots - flight path plots quickly generated from the GPS satellite data to verify the completeness and accuracy of a day's flying;
- Versatility - the FWS used in both the field and the office. Data pre-processed in the field up-loaded to the computers at the Data Processing Centre to speed up data turnaround;
- Preliminary Maps - the FWS software permitted creation preliminary maps of the electromagnetic and magnetic data during the survey;
- Quality Control – acquired data quickly and efficiently checked for quality in the field on daily basis.

6 Data Processing and Deliverables Specifications

6.1 MobileMT EM Data Processing

The MobileMT EM data processing procedures are described in Appendix II.

The frequencies extracted for data processing for the surveyed block are based on signal strength and local noise interference. The selected frequencies for the survey are presented in Table 7.

6.2 MobileMT Apparent Conductivity Axes Anomalies Tracing

The anomalies axes (from the inverted resistivity data) are traced based on the algorithm of adaptive one-dimensional energy filtering, which allows for optimal estimation of the parameters of informative and correlated signals with various spectral-correlation characteristics (Nikitin and Petrov, 2008). The adaptive energy filtering is executed on apparent conductivity grids for selected frequencies, and the results are combined into one map (example on Figure 6).

The next steps are executed in the procedure:

- The autocorrelation function is calculated across grids' rows to determine the correlation characteristics of the most energy-intensive (typically the most extended) anomalies on the rows;
- Based on the correlation radius, the size of the basic window of the adaptive filter is selected;
- For each point of the grid, within the vicinity of the basic filtering window, a standard filtering procedure is carried out.
- The autocorrelation function is calculated, the width and weighting coefficients of the filter are determined, and the initial field is convolved with the filter's weighting coefficients.
- The result of the convolution is assigned to the central point of the basic window, then the basic window is shifted by one point along the grid’s row, and the procedure is repeated for all rows of the grids.

As a result of the adaptive energy filtering, axes of conductive and resistive anomalies are presented in a separate map over distribution of magnetic field color grid (Appendix III).

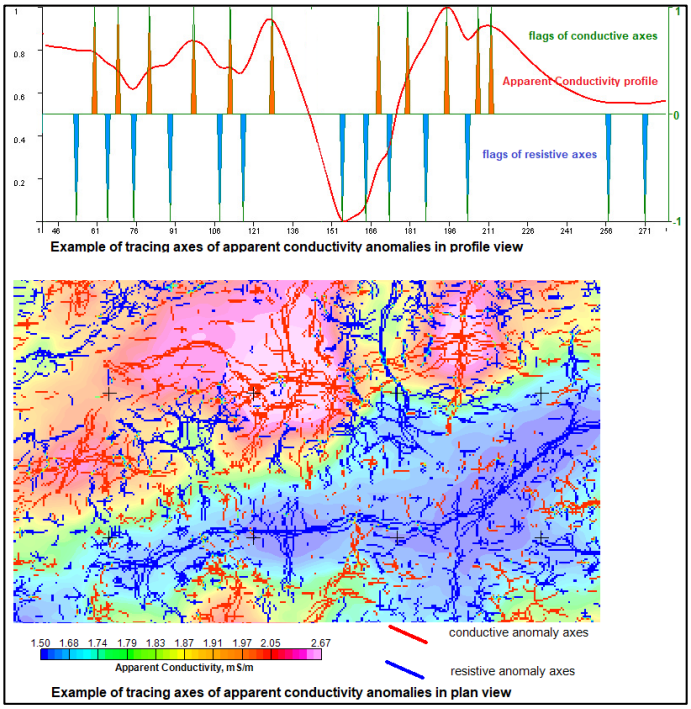


Figure 6 – Example of tracing axes of apparent conductivity anomalies in profile and plan view.

6.3 MobileMT EM Data Inversions

MobileMT electromagnetic data were inverted along all survey lines using the 2021 version of MARE2DEM, an open-source finite-element modelling and inversion code (Key, 2016). The workflow follows the approach described by Prikhodko et al. (2025), which adapts MARE2DEM to the MobileMT measurement configuration, combining airborne magnetic-field measurements with electric-field measurements at a stationary ground base station.

The inversion uses a 2.5D formulation: resistivity varies laterally and vertically within the model section and is assumed invariant perpendicular to it, while the electromagnetic fields are treated in three dimensions. This approach provides an efficient means of recovering resistivity structure along survey lines, particularly where the lines cross geological features that are approximately continuous along strike. Structures with substantial variation perpendicular to the section may require additional modelling or 3D inversion.

MARE2DEM uses unstructured triangular meshes and adaptive finite-element calculations to represent the terrain and subsurface resistivity distribution. Parallel processing supports efficient inversion of large airborne datasets. Its regularized, nonlinear inversion balances agreement with the observations against model roughness, favouring smooth resistivity distributions unless additional complexity is required by the data.

The workflow comprised data preparation and conversion to MARE2DEM input format, mesh generation, iterative inversion, assessment of data fit, and export of the resulting resistivity models to Geosoft databases and sections. The model meshes contained thousands of cells per line. Figure 7 illustrates an unstructured mesh along a survey-line segment, with triangular elements following the terrain surface and a finer discretization within the principal investigation interval. Larger elements outside this interval reduce computational requirements.

The inversions started from a uniform half-space model, without imposed geological constraints, while retaining the regularization required to stabilize the solution. Inversion quality was assessed using RMS misfit and comparisons between observed and calculated responses. Figure 8 compares observed apparent resistivity values (points) with modelled responses (lines) along a survey-line segment at multiple frequencies, illustrating how well the model reproduces lateral variations. Figure 9 presents the corresponding comparison in the frequency domain for selected stations, showing agreement with both the magnitude and shape of the apparent resistivity curves. Together, these comparisons assess the spatial and spectral consistency of the model, although a close fit does not establish a unique geological solution.

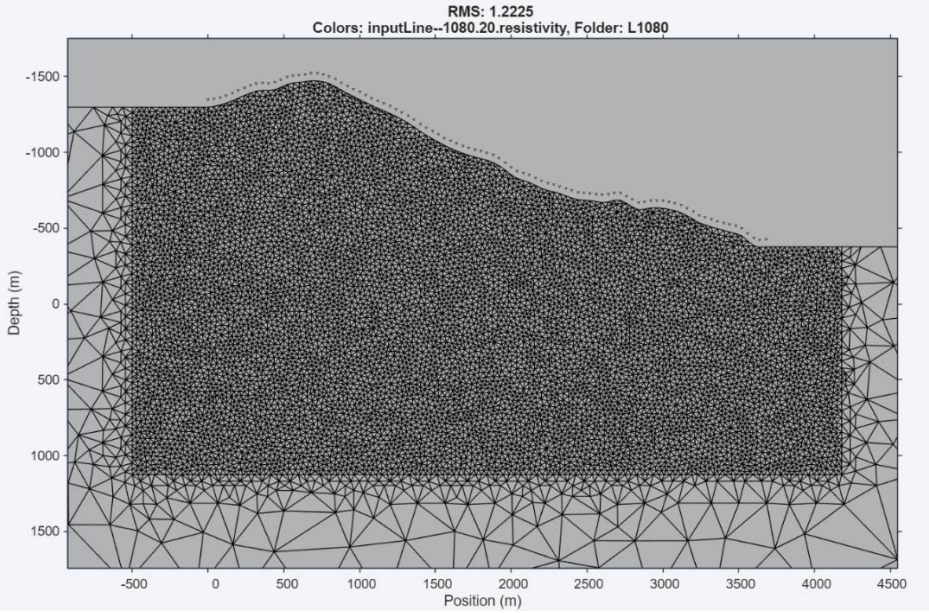


Figure 7 – Example of unstructured model mesh used as input to 2D inversions along a line segment of the survey.

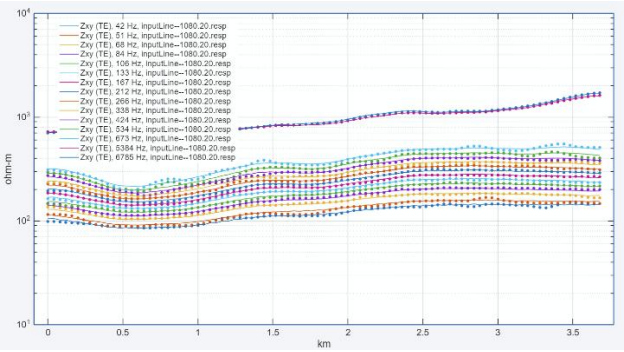


Figure 8 – Agreement between observed (points) and modelled (lines) apparent resistivity profiles along a line segment of the survey.

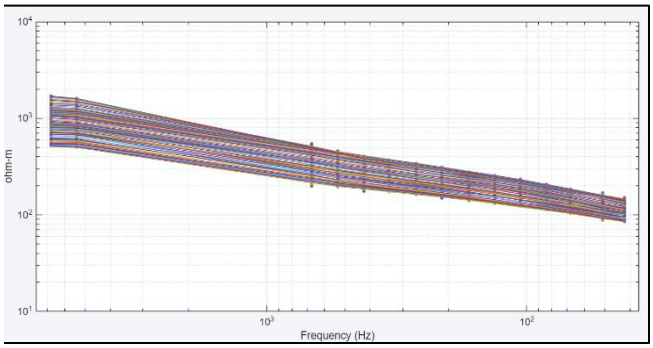


Figure 9 – Agreement between observed (points) and modelled (lines) apparent resistivity curves for stations along a line segment of the survey.

6.4 Magnetic Data Processing

Raw total magnetic field data are recorded at 0.1-second sampling intervals. The Earth's magnetic field is known to vary as a function of time. Time varying magnetic events such as magnetic storm transients and more regular diurnal variations which occur during the acquisition of magnetic data may affect the accuracy of the survey data and distort magnetic anomalies. Separation of the time-dependent variations in the magnetic field from a real geomagnetic anomaly requires an independent estimate of the transient magnetic field events. Base station magnetometer data provides this independent estimate. The diurnal base station data was analyzed for spikes and spurious sections which were manually removed from the dataset. A 20-point low pass filter was then applied to the diurnal data.

The magnetic data was corrected for diurnal variations, leveled, and filtered. Raw magnetic data has initial preprocessing only (spike removal, short gaps interpolated). At the next stage, all the magnetic data is processed by an adjustment procedure that statistically treats the line data. It is designed to recognize and remove systematic bias and small random errors in the data which can cause survey line mis-ties. Bias errors in the magnetic data arise from changes in the level of the total magnetic field.

To remove bias errors, each profile of a given data set in the survey was shifted up or down systematically by an amount such that the sum of the square of the mis-tie errors for that data set over the entire survey network is minimized. The systematic corrections are further constrained such that the sum of the systematic corrections is zero, effectively eliminating DC shifts to the network as a whole. After this systematic adjustment, the remaining intersection mis-ties were studied and removed. The final statistical choice of the data values at each intersection is a function of the reliability weights of each line for each data set. The random error correction for each data set prorated between

intersections. After editing the adjusted line data for line pulls and data quality, they were input to a minimum curvature gridding algorithm and a grid produced.

As an additional product, the calculated vertical gradient of total magnetic intensity (CVG-TMI) was produced.

6.5 Magnetic Field Data Inversions

The 2D inversion of magnetic field data was performed for all surveyed lines using the **MI2Dmp** program. The inverse problem in the software is solved using the gradient descent method with variable rate, similar to that described for the gravity field (Chepigo L. S., Lygin I.V., Bulychev A.A.: Gravity inverse problem solution with variable rate of gradient descent. Geophysical Research, 2022, vol. 23, no. 1, pp.5-19.)

The input file contains anomalous magnetic field data (without the regional field background) along survey lines. The inversion is executed using specified calculation parameters (configuration file) to derive a distribution of magnetic susceptibility. The output of the inversion results includes an ASCII and binary (grid) files. During the inversion, the program minimizes the discrepancy between the observed and calculated magnetic field:

$$L = \sqrt{\frac{\sum_{i=1}^{N}(\Delta T_{obs\,i} - \Delta T_{calc\,i})^2}{N}} \rightarrow min,$$

where $\Delta T_{obs\,i}$ – measured total magnetic field intensity with subtracted regional background on a measurement station i, $\Delta T_{calc\,i}$ – Calculated total magnetic field intensity from a theoretical model of magnetic susceptibility, N – number of measurement stations along a survey line.

The inversion is performed independently for each survey line. During the inversion, a gridded model of magnetic susceptibility is constructed using a regular mesh of rectangular cells. All model cells have the same length and height specified in the configuration file, except for those intersecting the topography.

6.6 VLF Data Processing

VLF data were captured using the MobileMT three components receiver. The instrument is capable of recording amplitude (total field) for multiple VLF frequencies. Amplitude is calculated as a vector sum of three orthogonal components (total field).

For this project, the following VLF transmitters were monitored:

- Station RDL: Krasnodar, Russia - 18.10 kHz
- Station HWU: Rosnay, France - 18.30 kHz
- Station NWC: Exmouth, Western Australia - 19.80 kHz
- Station NPM: Lualualei, Hawaii, USA - 21.40 kHz
- Station NPM: Lualualei, Hawaii, USA - 21.40 kHz
- Station NAA: Cutler, Maine, USA - 24.00 kHz
- Station NLK (Jim Creek): Seattle, Washington (USA) - 24.80 kHz
- Station LaMoure - Omega Station D: LaMoure, North Dakota, USA - 25.20 kHz

The 19.80, 24.00, and 24.80 kHz signals for Ajax were accepted and presented in the final database.

Processing of the raw amplitude data consisted of the following:

- Mask out any embedded “off-line” data
- Noise reduction filtering using non-linear Naudy filtering
- Initial levelling (mean subtraction)
- Fine levelling (micro-levelling)

The finalized data for accepted frequency(s) were presented as a series of amplitude colour images. High amplitude values correspond to conductive zones.

6.7 Ancillary Data Processing

Positions and altitudes of the magnetic sensor and EM receiver are derived from data of two GPS antennas (A – on the helicopter, B- on the magnetic sensor bird) and radar-altimeter positioned on the helicopter. A digital terrain model (DTM) channel has been calculated by subtracting the filtered radar-altimeter data from the GPS-A elevation.

6.8 Data Deliverables

EM Database: Ajax Block EM presented in Geosoft GDB format

- The database channels description is in Table 8.

Table 8 – Geosoft 26132_Ajax_EM.gdb Data Format

Channel Name	Units	Description
xe	m	EM bird UTM Easting WGS 84 UTM zone 9N
ye	m	EM bird UTM Northing WGS 84 UTM zone 9N
ze	m	EM bird elevation above geoid
gtime	Sec of the day	GPS time
RdAlt	m	helicopter terrain clearance from radar altimeter
alt_e	m	EM bird terrain clearance

Channel Name	Units	Description
DTM	m	Digital Elevation Model
PLM	Units	Powerline monitor
ac_33	mS/m	Apparent conductivity for freq 33.0 Hz
ac_42	mS/m	Apparent conductivity for freq 42.0 Hz
ac_51	mS/m	Apparent conductivity for freq 51.0 Hz
ac_68	mS/m	Apparent conductivity for freq 68.2 Hz
ac_84	mS/m	Apparent conductivity for freq 84.0 Hz
ac_106	mS/m	Apparent conductivity for freq 105.9 Hz
ac_133	mS/m	Apparent conductivity for freq 133.4 Hz
ac_167	mS/m	Apparent conductivity for freq 167.3 Hz
ac_212	mS/m	Apparent conductivity for freq 211.9 Hz
ac_266	mS/m	Apparent conductivity for freq 266.0 Hz
ac_338	mS/m	Apparent conductivity for freq 338.2 Hz
ac_424	mS/m	Apparent conductivity for freq 424.4 Hz
ac_534	mS/m	Apparent conductivity for freq 534.1 Hz
ac_673	mS/m	Apparent conductivity for freq 673.4 Hz
ac_4274	mS/m	Apparent conductivity for freq 4273.7 Hz
ac_5384	mS/m	Apparent conductivity for freq 5384.0 Hz
ac_6785	mS/m	Apparent conductivity for freq 6784.9 Hz
ac_8550	mS/m	Apparent conductivity for freq 8549.8 Hz
ac_10772	mS/m	Apparent conductivity for freq 10772.1 Hz
ac_13572	mS/m	Apparent conductivity for freq 13571.7 Hz

The EM and MAG databases can be synchronized based on *gtime* channel.

Mag Database: Ajax Block Mag presented in Geosoft GDB format

- The database channels description is in Table 9

Table 9 – Geosoft 26132_Ajax_Mag.gdb Database Format

Channel Name	Units	Description
xm	m	mag bird UTM Easting WGS 84 UTM zone 9N
ym	m	mag bird UTM Northing WGS 84 UTM zone 9N
zm	m	mag bird elevation above geoid
xh	m	heli UTM Easting WGS 84 UTM zone 9N
yh	m	heli UTM Northing WGS 84 UTM zone 9N
zh	m	heli elevation above geoid
gtime	Sec of the day	GPS time
RdAlt	m	helicopter terrain clearance from radar altimeter
alt_m	m	mag bird terrain clearance
DTM	m	Digital Terrain Model
GPS_B_LAT	Decimal degrees	Mag bird latitude, WGS 84
GPS_B_LON	Decimal degrees	Mag bird longitude, WGS 84
basemag	nT	Magnetic base station data
Magair	nT	Measured magnetic field
Magcorr	nT	Magnetic field corrected for diurnal magnetic field

Channel Name	Units	Description
TMI	nT	Total magnetic intensity, levelled and microlevelled
CVG_TMI	nT/m	Calculated vertical derivative of the magnetic field

The EM and MAG databases can be synchronized based on *gtime* channel.

VLF Database: Ajax Block VLF presented in Geosoft GDB format

- The database channels description is in Table 10.

Table 10 – Geosoft 26132_Ajax_VLF.gdb Database Format

Channel Name	Units	Description
xe	m	EM bird UTM Easting WGS 84UTM zone 9N
ye	m	EM bird UTM Northing WGS 84UTM zone 9N
ze	m	EM bird elevation above geoid
gtime	Sec of the day	GPS time
alt_e	m	EM bird terrain clearance
DTM	m	Digital Elevation Model
Amplitude_3	units	VLF total field amplitude for freq 19.80 kHz
Amplitude_6	units	VLF total field amplitude for freq 24.00 kHz
Amplitude_7	units	VLF total field amplitude for freq 24.80 kHz

Grids and Maps:

- Refer to Table 11 for summary of grids and maps (Appendix III) which accompany this report.

Table 11 – List of Ajax Block grids (in Geosoft format) and maps (in Geosoft and PDF formats).

Grids	Maps	Description
DTM	26132_Ajax_DTM	Digital Elevation Model
TMI	26132_Ajax_TMI	Total magnetic intensity, levelled and microlevelled
CVG_TMI	26132_Ajax_CVG_TMI	Calculated vertical derivative of the magnetic field
VLFAmplitude_3	26132_Ajax_VLFAmplitude-3	Total field VLF amplitude at 19.80 kHz
VLFAmplitude_6	26132_Ajax_VLFAmplitude-6	Total field VLF amplitude at 24.00 kHz
VLFAmplitude_7	26132_Ajax_VLFAmplitude-7	Total field VLF amplitude at 24.80 kHz
ac_33		Apparent conductivity for freq 33.0 Hz
ac_42		Apparent conductivity for freq 42.0 Hz
ac_51		Apparent conductivity for freq 51.0 Hz
ac_68	26132_Ajax_ac_68	Apparent conductivity for freq 68.2 Hz
ac_84		Apparent conductivity for freq 84.0 Hz
ac_106		Apparent conductivity for freq 105.9 Hz
ac_133	26132_Ajax_ac_133	Apparent conductivity for freq 133.4 Hz
ac_167		Apparent conductivity for freq 167.3 Hz
ac_212		Apparent conductivity for freq 211.9 Hz
ac_266	26132_Ajax_ac_266	Apparent conductivity for freq 266.0 Hz
ac_338		Apparent conductivity for freq 338.2 Hz

Grids	Maps	Description
ac_424	26132_Ajax_ac_424	Apparent conductivity for freq 424.4 Hz
ac_534		Apparent conductivity for freq 534.1 Hz
ac_673		Apparent conductivity for freq 673.4 Hz
ac_4274	26132_Ajax_ac_4274	Apparent conductivity for freq 4273.7 Hz
ac_5384		Apparent conductivity for freq 5384.0 Hz
ac_6785		Apparent conductivity for freq 6784.9 Hz
ac_8550		Apparent conductivity for freq 8549.8 Hz
ac_10772		Apparent conductivity for freq 10772.1 Hz
ac_13572		Apparent conductivity for freq 13571.7 Hz
	26132_Korestar_ac106-212Hz _traceAnoms	Axes of conductive and resistive apparent conductivity anomalies
ResDepth_XXXX	26132_Korestar_ResDepth_ XXX	Resistivity depth slices from 100m to 1300m below surface at 100m intervals
LXXX_Resistivity	LXXX	Resistivity Line Sections with full depth range
LXXX_Susceptibility	LXXX	Magnetic Susceptibility Sections plotted with full depth range

Voxels:

- 26132_Korestar_ResElev.geosoft_voxel

PDFs: Combined Magnetic Susceptibility and Resistivity Depth Sections for each line:

- 26132_Korestar_MagSusc_Res_Sections.pdf

Geoscience Analyst: Ajax project loaded as a workspace

Geoscience Analyst free viewer can be downloaded from https://www.mirageoscience.com

- Refer to Figure 10 for a sample of objects loaded to the workspace
- Figure 11 displays some examples of 2D Profiles / Slices and 3D data visualization options

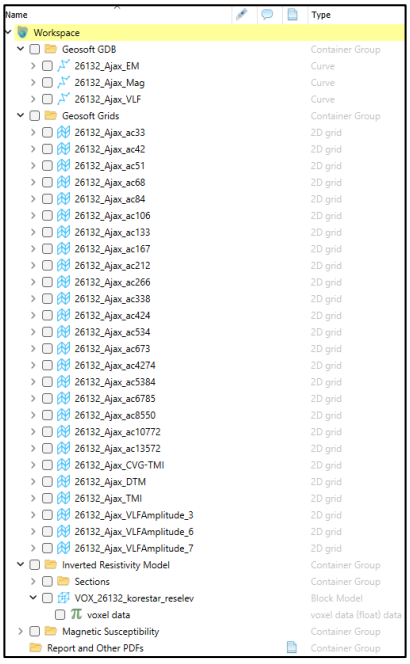


Figure 10 – Data types loaded into 26132_Ajax_GA Project.geoh5 Geoscience Analyst Workspace.

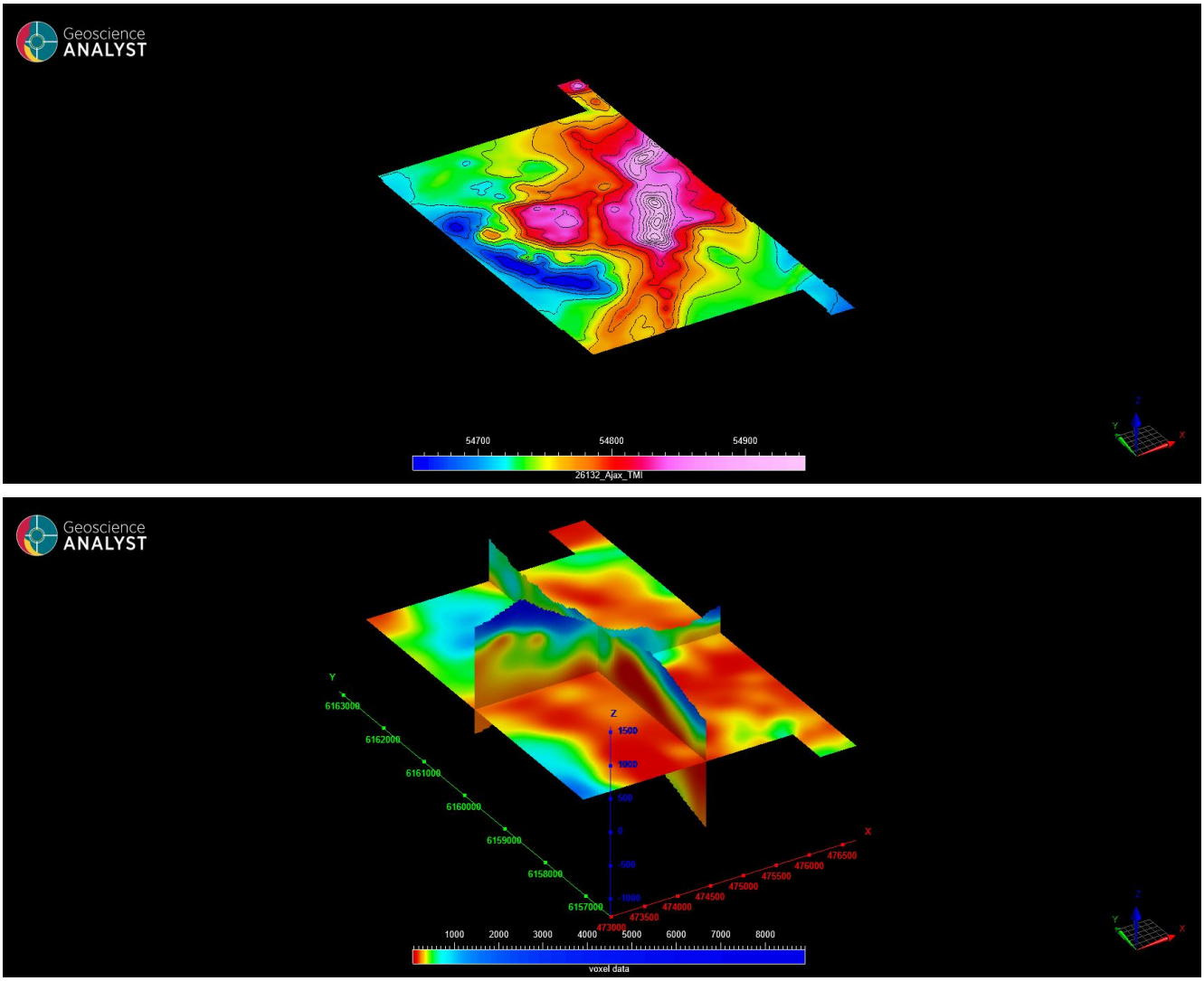


Figure 11 – Example of data visualization options in Geoscience Analyst (top: plan map of TMI grid; Bottom: Voxel slices and section image)

7 Survey Results General Analysis and Recommendations

A MobileMT airborne survey, including broadband natural electromagnetic fields, the earth's magnetic field, and EM VLF data measurements with precise positioning, has been successfully completed across the MobileMT Ajax block. Electromagnetic and magnetic data were collected along N-S (N 0° E) survey lines nominally spaced at 100 m, and tie lines are oriented perpendicular to the survey lines and spaced at 1000 m. Electromagnetic readings were taken using an EGL AFMAG&VLF MobileMT system consisting of an airborne three-component magnetic sensor, as well as a base station with two horizontal electric components. A caesium vapour magnetometer in a separate towed-bird was used for collecting measurements of the intensity of the earth's magnetic field.

Geological Context and Mineralization

The Ajax MobileMT survey block is situated at the southern end of the Golden Triangle mineral belt in northwestern Stikine terrane of the Canadian Cordillera in BC (Figure 12). The Stikine volcanic island arc terrane encompasses three unconformity-bounded volcano-sedimentary successions: the Paleozoic Stikine assemblage, the Upper Triassic Stuhini Group, and the Upper Triassic to Middle Jurassic Hazelton Group (Nelson et al., 2018). In the region, the Stuhini Group consists of augite-phyric mafic volcanics and marine sedimentary rocks, which are unconformably overlain by intermediate volcanic and sedimentary strata of the Hazelton Group (Nelson et al., 2018). These stratified units are intruded by several coeval plutonic suites, including the Late Triassic Stikine, Galore, and Tatogga suites, the Early Jurassic Texas Creek suite (Nelson et al., 2018), and the younger Eocene Hyder plutonic suite (Alldrick, 1993). Regional deformation occurred during the mid-Cretaceous with the development of the Skeena fold-and-thrust belt, which drove northeasterly directed shortening across the central Intermontane belt via sinistral transpression (Evenchick et al., 2007). By the middle to Late Cretaceous, a shift in relative plate motions from sinistral to dextral kinematics initiated large-scale dextral faulting (Nelson et al., 2013). This transition was followed by Paleocene to Eocene dextral-transtensional tectonics, which accommodated significant offset along pre-existing orogen-parallel structures (Nelson et al., 2013).

The Ajax survey block is predominantly underlain by Late Triassic sedimentary and volcanic successions of the Stuhini Group, comprising well-stratified argillites, mudstones, siltstones, wackes, and feldspathic sandstones, alongside massive-to-stratified mafic coherent units, mafic volcanic

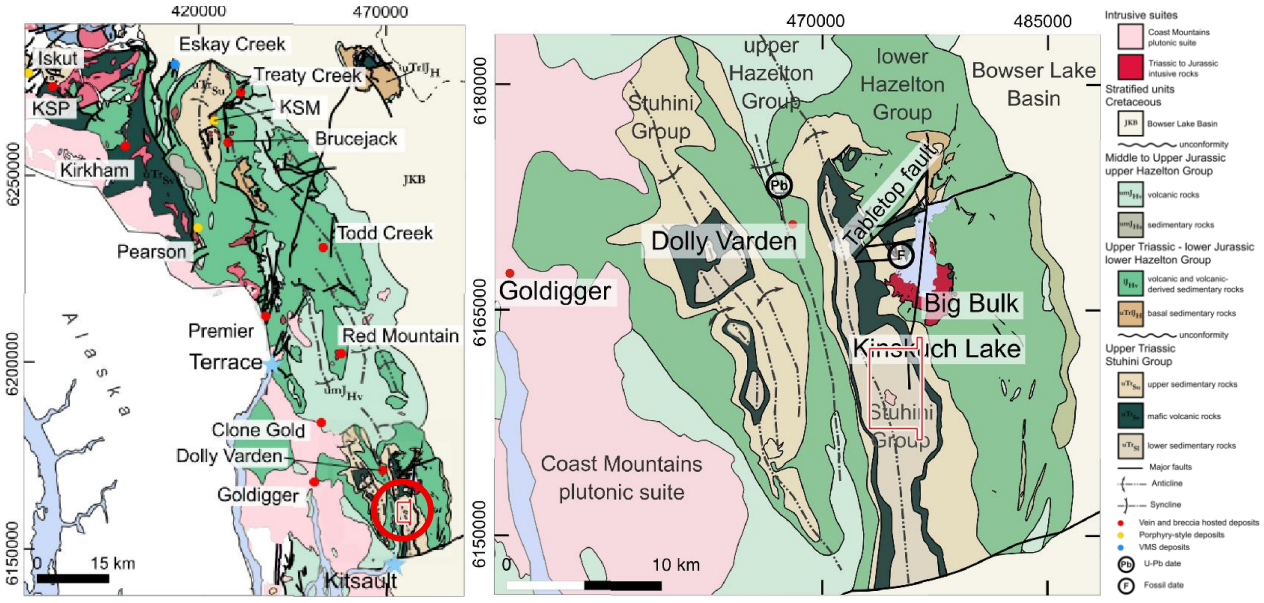


Figure 12 – left: Regional geologic map of the northwestern Stikinia Terrane with Cu(±Au±Mo) porphyry (yellow) and vein and breccia-hosted (including epithermal) deposits (red; Colpron and Nelson, 2011) and right: a close-up simplified geologic map of the Ajax MobileMT survey block (outlined in red) with locations of nearby deposits (modified after Miller et al., 2020)

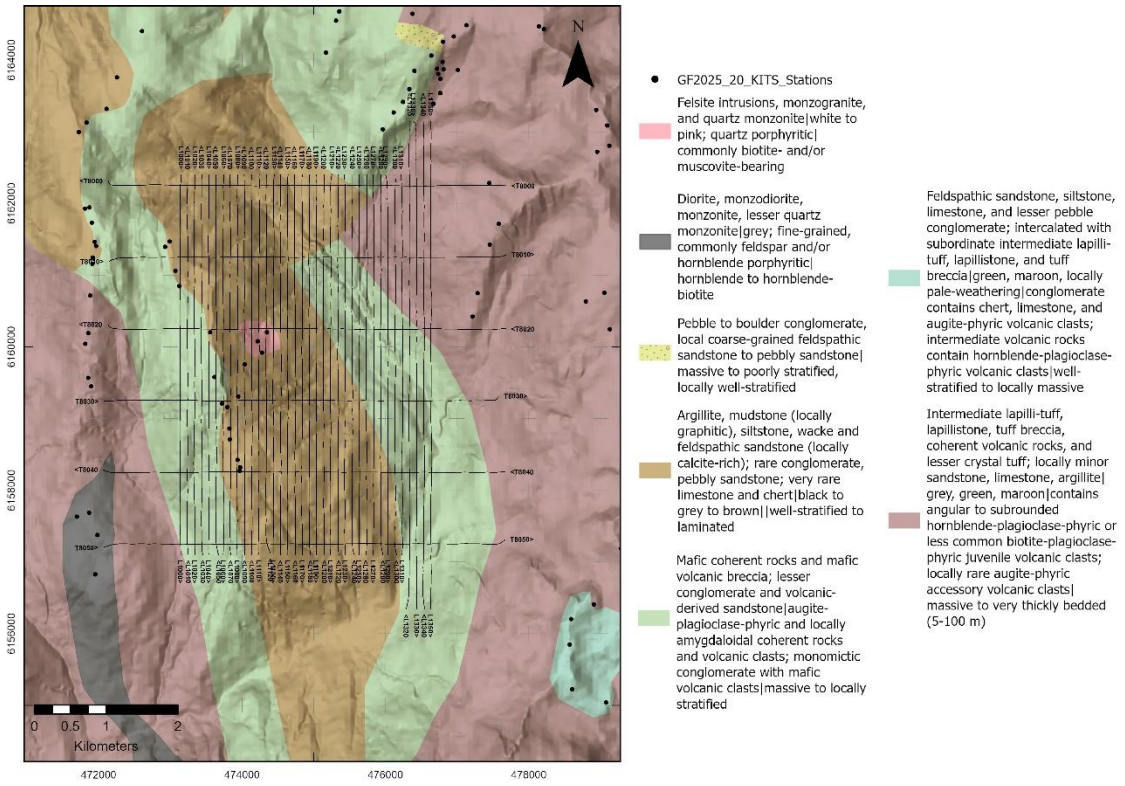


Figure 13 – Geologic map of the survey area with the Ajax MobileMT survey lines.

breccias, minor conglomerates, and volcaniclastic sandstones. The northeastern portion of the block is unconformably overlain by the intermediate lapilli-tuffs, lapillistones, and tuff breccias of the lower Hazelton Group's Betty Creek Formation. These sequences are subsequently cut by felsic to intermediate intrusions of the Eocene Alice Arm intrusive suite, including felsites, monzogranites, and quartz monzonites (Figure 13).

The Golden Triangle is a world-class mineral district believed to had been formed by tectonic subduction and arc volcanism between 220 and 175 Ma. It hosts significant deposits such as Eskay Creek, Brucejack, KSM, and Red Chris (Figure 12). One of the most notable deposit in the district was Eskay Creek which was Canada's highest grade Au mine and the world's fifth largest Ag producer, with production well over 3 million ounces of gold and 160 million ounces of Ag. Regional Cu-Au mineralization is strongly localized along the "Red Line", which is the the key stratigraphic contact between Triassic Stuhini Group and Jurassic Hazelton Group rocks. Porphyry copper-gold deposits, epithermal Au-Ag veins, and volcanogenic massive sulphide (VMS) systems coexist in the region, often in clusters. The Ajax property hosts a prominent molybdenum porphyry prospect tested by 48 historical drill holes since the mid-1960s. The property is located approximately 12 km south-southeast of Dolly Varden Silver, 7 km south of Big Bulk, and 17 km east of Goliath Resources' Golddigger/Surebet property (Figure 12) and is located within 1-3km from the Red Line. The 2023 exploration program on Ajax Property evaluated peripheral quartz vein systems extending 800 m upslope from the porphyry zone, returning high-grade gold results up to 37.89 g/t Au, along with elevated tungsten, antimony, and bismuth pathfinder elements.

Basic geophysical data analysis

The purpose of the survey was to map bedrock structures and lithology, including possible alteration and mineralization zones reflected in the electrical and magnetic properties of rocks. The airborne geophysical survey results are presented as apparent conductivity corresponding to different frequencies, resistivity-depth profiles determined from inverting EM data, available VLF data, as well as magnetic field data and its derivatives. The report is followed by digital databases, separate for each method, processed and calculated data grids, maps, and resistivity-depth products – elevation slices, sections, and a 3D voxel representation. The standard EM data inversion was based on a 2.5D model (2D geological structures and 3D primary EM field).

The electrical properties of the rock assemblages in the survey area are reflected in the distribution of apparent conductivities related to different frequencies and in the inverted resistivity-depth distributions. The apparent conductivity parameter describes an inhomogeneous geoelectrical environment in terms of a homogeneous earth that would produce the same measurement and refers to the depth relative to total conductance below the measurement station and a specific frequency. In general, depth of investigation increases with decreasing frequency and total resistance. The non-linear and complex relation is solved by inversions of the 'apparent conductivity - frequency' data into 'resistivity – depth' distributions.

The overall resistivity distribution of the Ajax survey block is presented in a 3D resistivity voxel (Figure 14). The voxel, when displayed with a single color distribution that considers the full resistivity range of the block, may appear to lack fine details. To better visualize more subtle resistivity contrasts it is recommended to analyze each section independently, as they offer more detail by using a color distribution statistically adjusted to the resistivity range for each line. A map of apparent conductivity at 133 Hz overlapped with contours of magnetic anomalies derived from the total magnetic intensity is provided in Figure 15. Magnetic field distribution and its vertical derivative are presented in corresponding maps following the report and in Appendix III. In general, the major conductive anomalies in the west portion are spatially associated with relatively lower magnetic response. (Figure 15). Behavior of the resistive and conductive zones with depth are shown in resistivity sections following the report.

The structural analysis results show conductive and resistive axes extracted from a series of apparent conductivity values in a specified data frequency range over the total magnetic intensity colour grid (Figure 16).

The lateral and in-depth distribution of the resistive and conductive zones for the block are presented in the resistivity-depth slices (Appendix III).

Examples of three magnetic susceptibility and corresponding resistivity sections along the lines crossing historic drillholes are shown in Figure 17, Figure 18 and Figure 19.

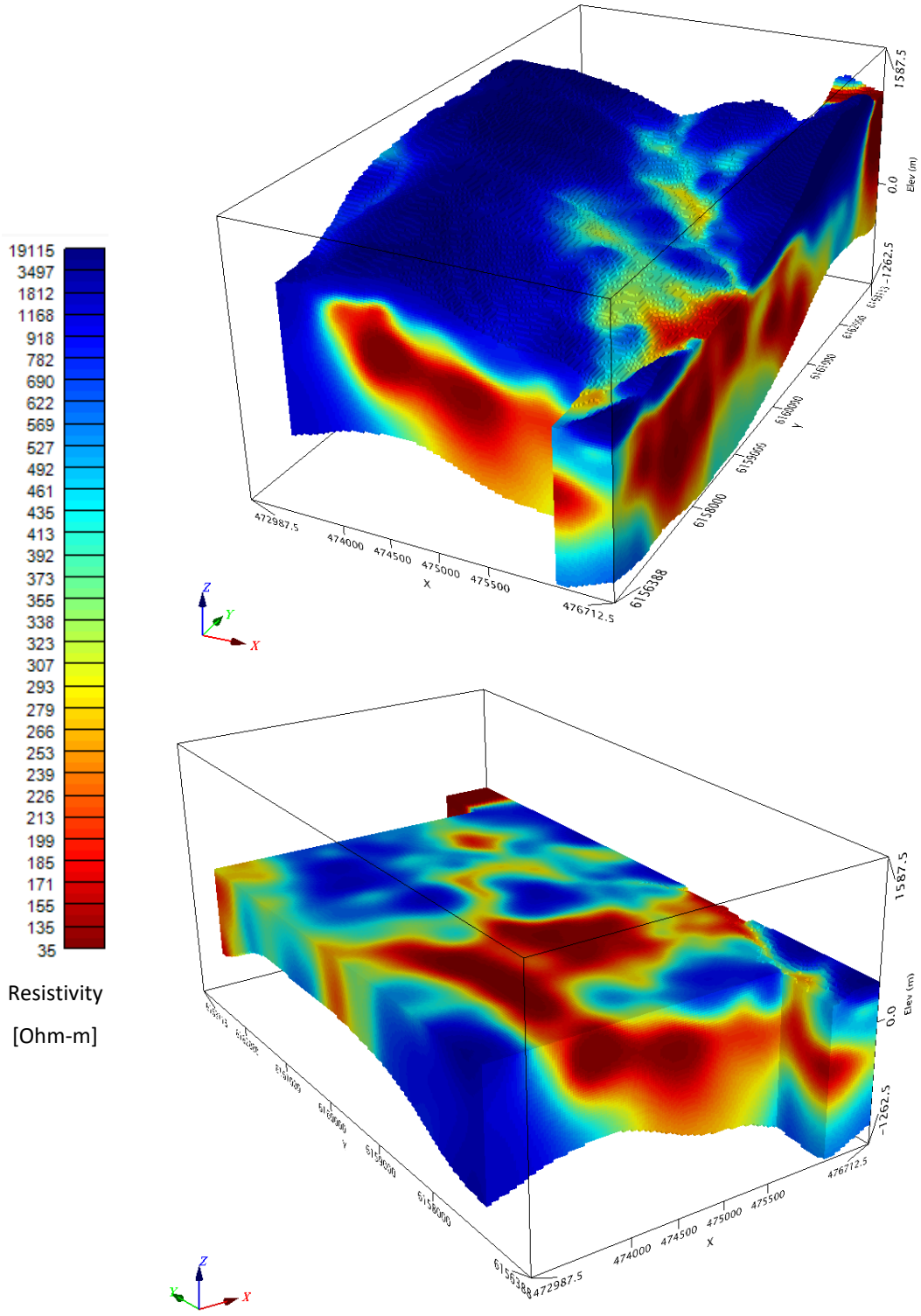


Figure 14 – Resistivity voxel in 3D view. Top: at surface, bottom: at 400 m ASL.

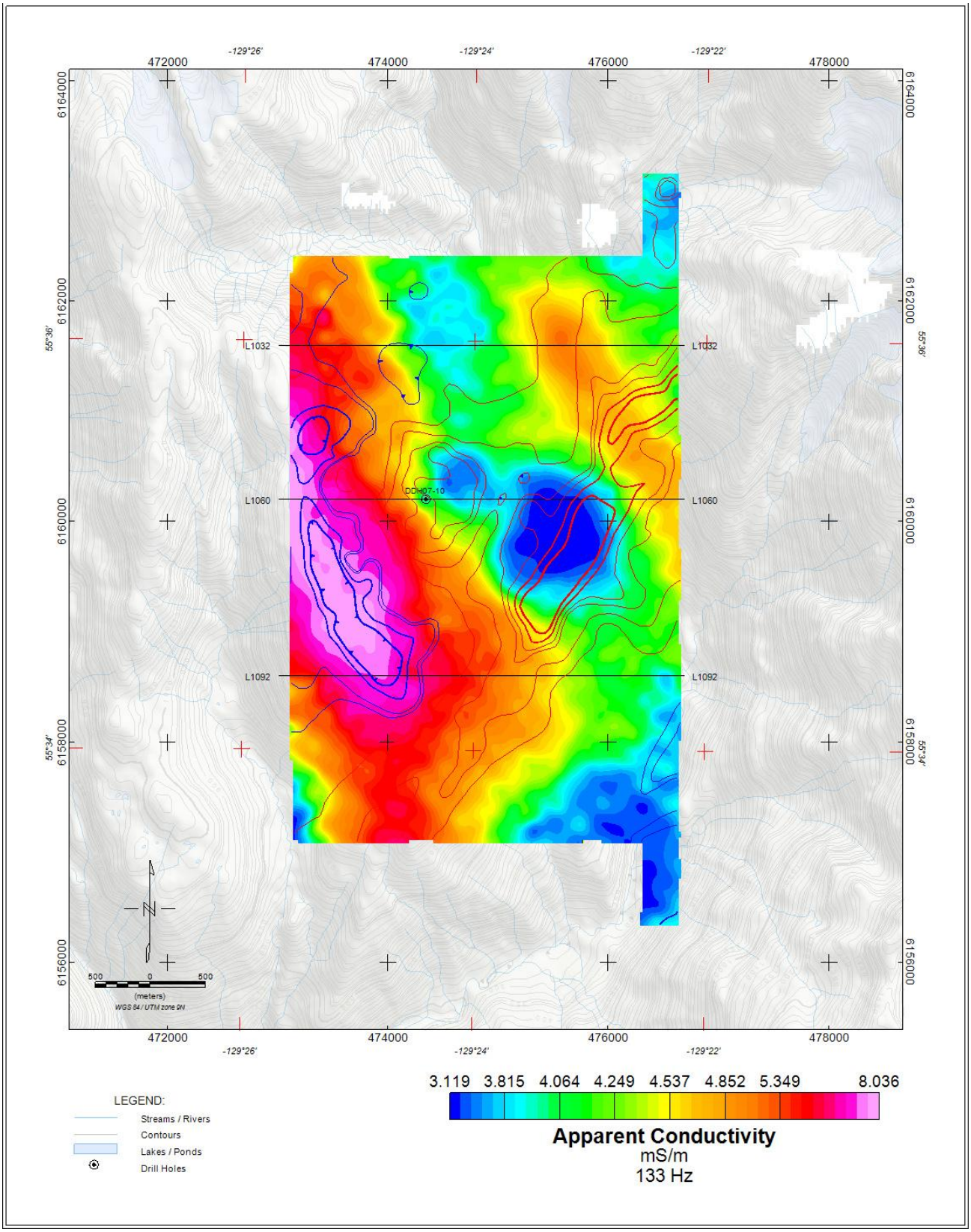


Figure 15 – Apparent conductivity (133 Hz) color grid with overlapped contours total magnetic intensity anomalies.

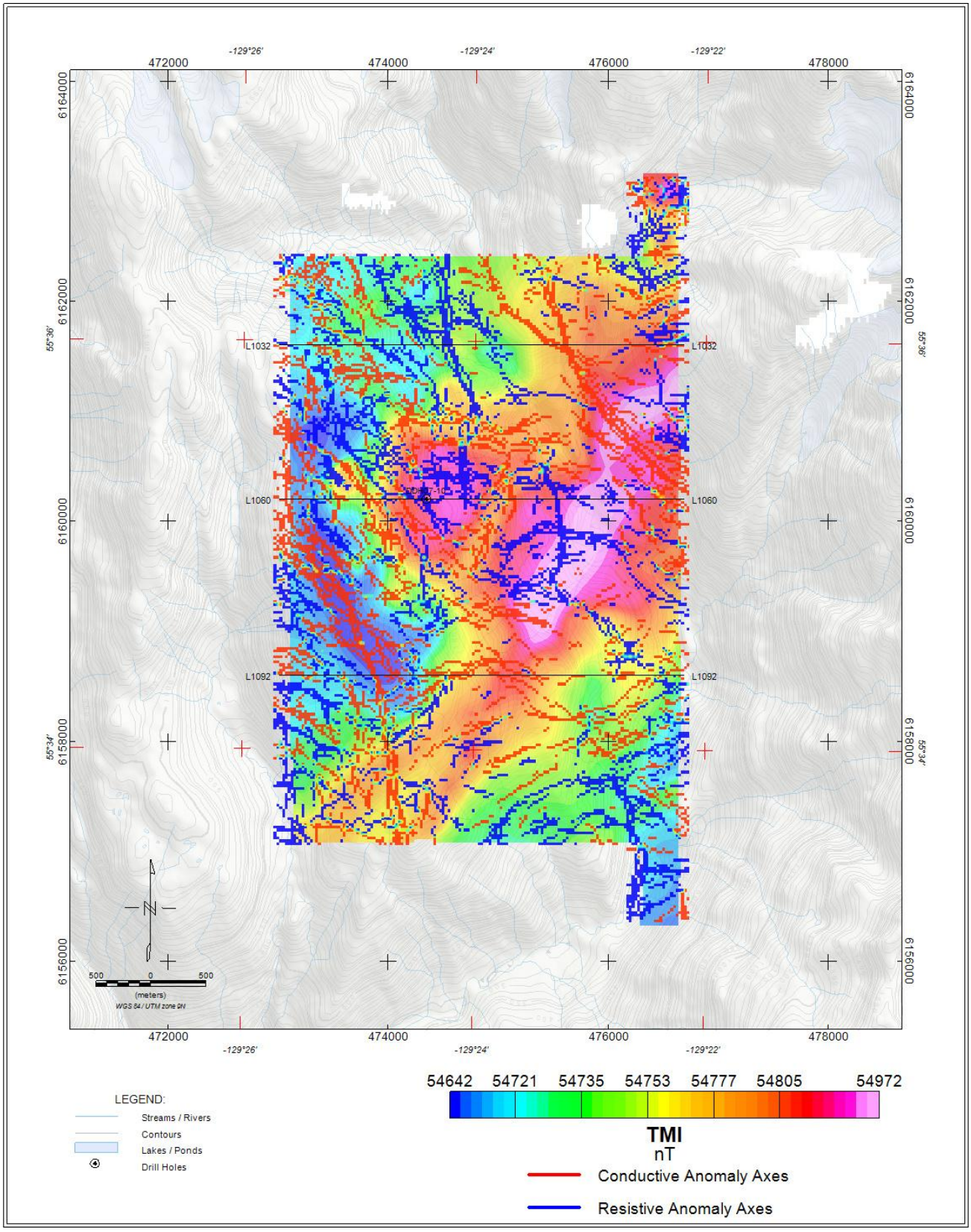


Figure 16 – Apparent conductivity anomalies axes from 106-212 Hz data over total magnetic intensity

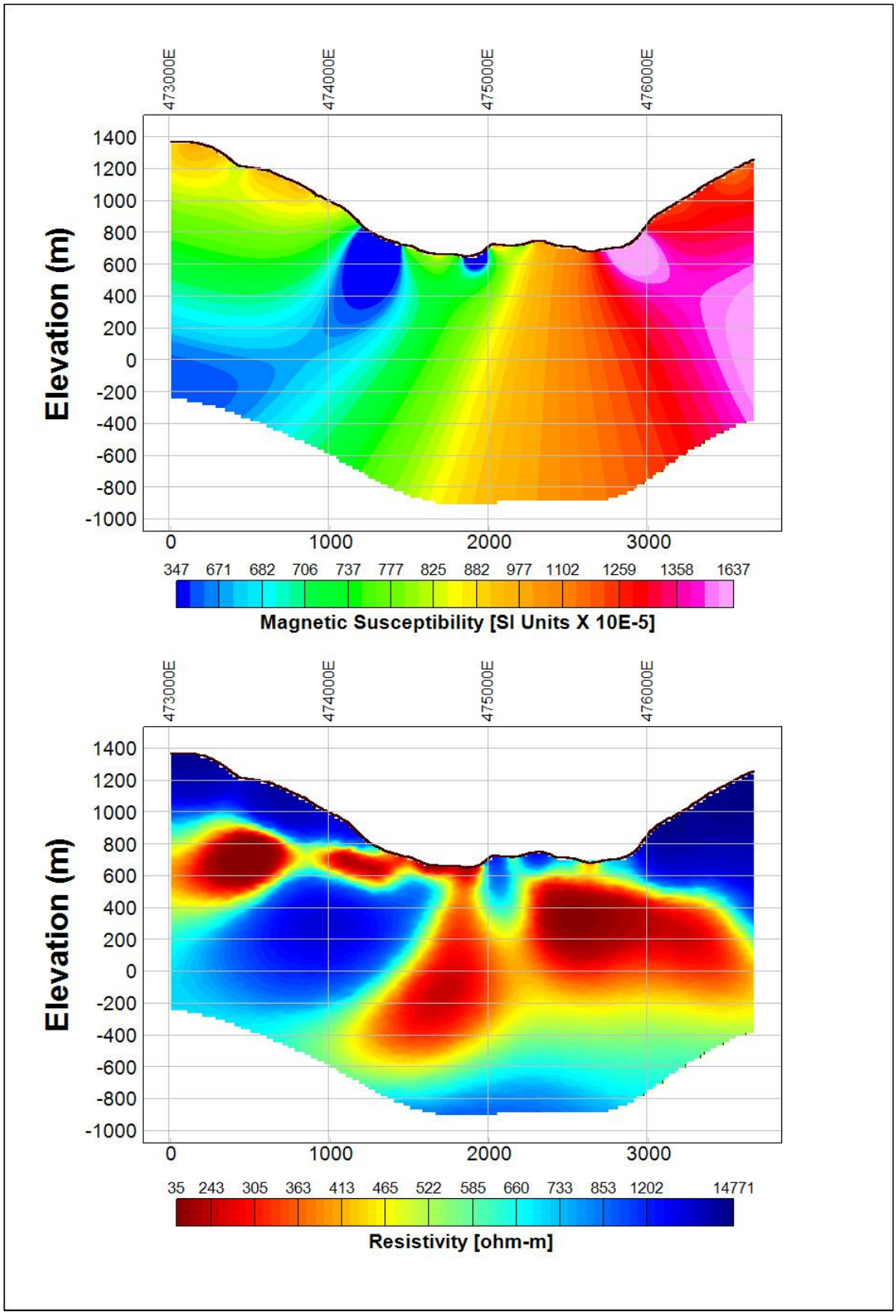


Figure 17 – Magnetic Susceptibility (top) and Resistivity (bottom) sections along L1032 (location shown in Figure 15). Sections shown from W → E. Locations of drillholes are marked.

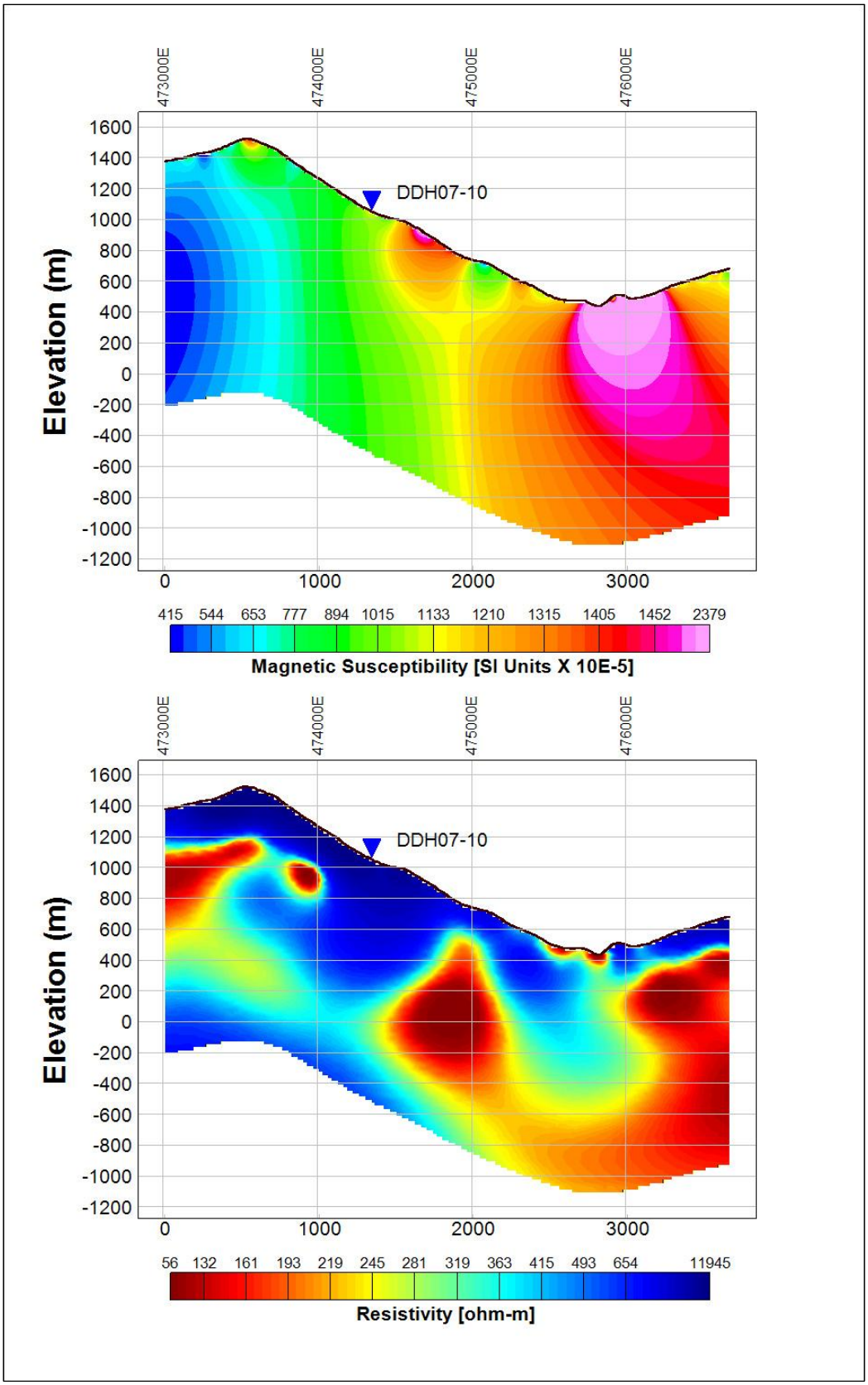


Figure 18 – Magnetic Susceptibility (top) and Resistivity (bottom) sections along L1060 (location shown in Figure 15). Sections shown from W → E. Locations of drillholes are marked.

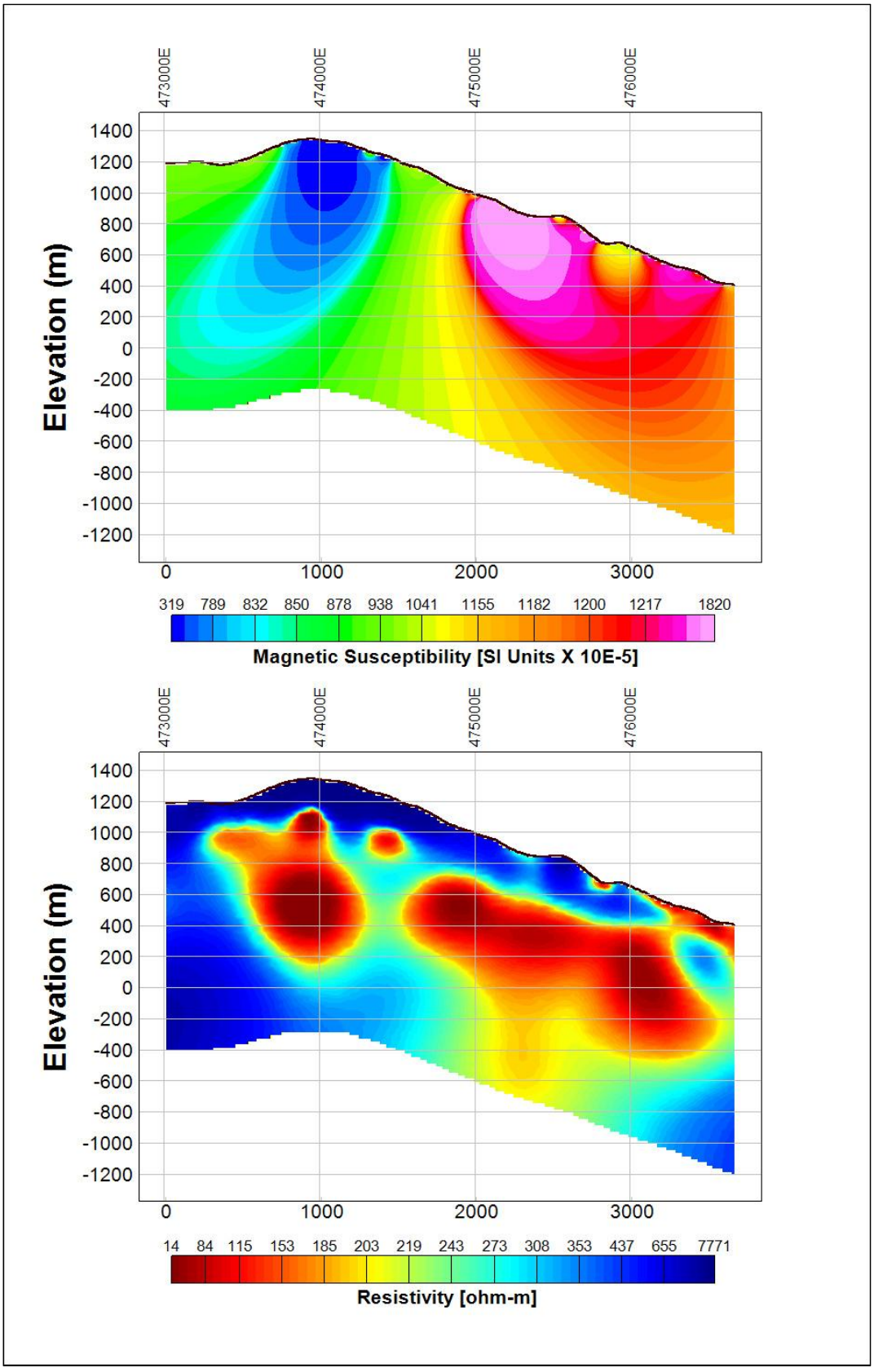


Figure 19 – Magnetic Susceptibility (top) and Resistivity (bottom) sections along L1092 (location shown in Figure 15). Sections shown from W → E. Locations of drillholes are marked.

8 Conclusions and Recommendations

Conclusions

The helicopter-borne MobileMT electromagnetic and magnetic survey over the Ajax block for Korestar Exploration Inc. was successfully completed, covering 230 line-km across 19 km^2. All planned lines were acquired and validated through field and office quality control. The survey produced high-quality broadband electromagnetic, VLF, and magnetic data, providing consistent coverage and reliable inversion results.

The main digital products in the result of the survey include databases, voxel, sections, depth slices, grids, geotiffs, and maps of resistivity, apparent conductivity, VLF amplitudes, and magnetic products.

All inputs referenced above are provided in the final deliverables for immediate use in GIS/Geosoft workflows. All pictures in the report are presented as examples, the full set of digital data follow the report in corresponding files and archives.

The main geophysical survey goals at Ajax Block achieved:

- Successful delineation of the principal conductive and resistive geophysical domains within the Ajax survey area through the integration of MobileMT resistivity, apparent conductivity, magnetic, and VLF datasets. The survey improved the understanding of lithological variability, intrusive contacts, and possible alteration-related geoelectrical contrasts associated with the local volcanic-sedimentary and intrusive rock packages.
- Integration of apparent conductivity, resistivity inversion, and magnetic data identified multiple conductivity gradients, resistivity contrasts, and structurally complex zones that may reflect lithological contacts, faulting, hydrothermal alteration, and sulphide-bearing geological units. Several of these features occur within areas of historical exploration activity and provide valuable constraints for follow-up geological interpretation and target evaluation.
- The 2.5D Mare2DEM inversion results and the derived 3D resistivity voxel model improved the understanding of the geometry and depth extent of subsurface resistivity features within the surveyed area. While the survey coverage is limited and does not permit confident interpretation of property-scale structural trends, the results successfully highlighted several local areas of interest characterized by significant resistivity contrasts and structural complexity that warrant further investigation.

Overall, the survey successfully achieved its objective of providing high-resolution geophysical data to support exploration targeting within the survey block. The dataset highlights multiple anomalies that warrant further investigation, but additional work is required to assess their potential association with alteration zones or mineralization.

Recommendations

Based on the results of this survey, the following recommendations are made:

- Detailed analysis of all geophysical data MobileMT EM, VLF and magnetic in relation to an exploration model considered for the surveyed area and integrate these data with other available geological and geochemical information, for refining targets, follow-up ground work, and ultimately drilling planning.
- Target prioritization with ranking conductive trends and structural zones of interest by their geophysical response, geometry, and geological setting, and selecting anomalies or geophysical field features that spatially correlate with major structures or known mineralization trends in the area.
- Detailed data analysis over specific zones or anomalies of interest.

The inversions included as part of the deliverables are unconstrained in nature. For drilling purposes, detailed 3D inversions are recommended over selected anomalies or zones of interest. In areas of complex topography, 2D inversions may be limited by three-dimensional effects related to both rugged relief and geological structure, whereas 3D inversion provides a more appropriate basis for detailed target definition. Structural modeling based on lineament/trend analysis of inverted EM data will help to extract more details and precise positioning of the central parts of potential targets and structures.

9 References

Alldrick, D. J. (1993). Geology and metallogeny of the Stewart mining camp, British Columbia (Bulletin No. 85). British Columbia Ministry of Energy, Mines and Petroleum Resources.

Colpron, M., & Nelson, J. (2011). A digital atlas of terranes for the northern Cordillera (GeoFile 2011-11). British Columbia Ministry of Energy, Mines and Petroleum Resources, British Columbia Geological Survey.

Evenchick, C. A., McMechan, M. E., McNicoll, V. J., & Carr, S. D. (2007). A synthesis of the Jurassic-Cretaceous tectonic evolution of the central and southeastern Canadian Cordillera: Exploring links across the orogen. In J. W. Sears, T. A. Harms, & C. A. Evenchick (Eds.), Whence the mountains? Inquiries into the evolution of orogenic systems: A volume in honor of Raymond A. Price (Special Paper 433, pp. 117–145). Geological Society of America.

Key, K. (2016). MARE2DEM: A 2-D inversion code for controlled-source electromagnetic and magnetotelluric data. Geophysical Journal International, 207(1), 571–588. https://doi.org/10.1093/gji/ggw290

Miller, E. A., Kennedy, L. A., & van Straaten, B. I. (2020). Geology of the Kinskuch Lake area and Big Bulk porphyry prospect, northwestern British Columbia: Syndepositional faulting and basin formation during the Rhaetian (latest Triassic) transition from the Stuhini to the Hazelton Group. In Geological Fieldwork 2019 (Paper 2020-01, pp. 77–99). British Columbia Ministry of Energy, Mines and Petroleum Resources, British Columbia Geological Survey.

Nelson, J. L., Colpron, M., & Israel, S. (2013). The Cordillera of British Columbia, Yukon, and Alaska: Tectonics and metallogeny. In M. Colpron, T. Bissig, B. G. Rusk, & J. F. H. Thompson (Eds.), Tectonics, metallogeny, and discovery: The North American Cordillera and similar accretionary settings (Special Publication 17, pp. 53–109). Society of Economic Geologists.

Nelson, J., Waldron, J., van Straaten, B., Zagorevski, A., & Rees, C. (2018). Revised stratigraphy of the Hazelton Group in the Iskut River region, northwestern British Columbia. In Geological Fieldwork 2017 (Paper 2018-01, pp. 15–38). British Columbia Ministry of Energy, Mines and Petroleum Resources, British Columbia Geological Survey.

Nikitin, A. A., & Petrov, A. V. (2008). Theoretical foundations of geophysical information processing. Publishing House.

Prikhodko, A., Sirohey, A., & Philipovich, A. (2025). Advancing deep ore exploration with MobileMT: Rapid 2.5D inversion of broadband airborne EM data. Minerals, 15(8), Article 874. https://doi.org/10.3390/min15080874

Starcore International Mines Ltd. (2023, November 20). *Starcore completes 2023 exploration at its Ajax property, Golden Triangle area, British Columbia* [Press release]. https://starcore.com/starcore-completes-2023-exploration-at-its-ajax-property-golden-triangle-area-british-columbia/

Alexander Prikhodko, Ph.D., P.Geo



_____

October 29, 2026

MobileMT Job #26132 for Korestar Exploration Inc.



Appendix I Company Profile

About us

Expert Geophysics Surveys Inc. is based in Toronto, Canada.

President and founder, **Andrei Bagrianski**, Ph.D., P.Geo., has over 35 years of professional experience in the acquisition, processing, and interpretation of airborne and ground geophysical data for a wide range of applications. From 2002 to 2016, he was Chief Operating Officer and General Manager at Geotech Ltd. Andrei has been directly involved in contracting, organizing, and supervising hundreds of airborne geophysical surveys on all continents except Antarctica. Andrei has extensive international field work experience that includes projects in Australia, Brazil, Bolivia, Colombia, Ecuador, Peru, Botswana, Malawi, South Africa, Libya, USA, Canada, Russia, Kazakhstan, and India.

Petr Kuzmin, Ph.D., the designer of the **MobileMT** system, has over 40 years of experience in the development of ground and airborne TDEM, MT, and IP methods, equipment, and software. Working for Geotech Ltd., Canada, from 2000 until 2009, Dr. Kuzmin was the principal designer of the award winning systems VTEM, ZTEM, and AirMt. Since 2009, Dr. Kuzmin has completed a number of successful developments: ground AFMAG, ultra-fast airborne TD (HiRes), airborne VLF system, an airborne navigation system, a high accuracy magnetometer counter, and the MobileMT. Dr. Kuzmin holds a doctorate in Geophysics, has authored nearly 20 patents, and published over 40 technical papers.

Vice President and Chief Geophysicist, **Alexander Prikhodko**, Ph.D. in geoscience, P.Geo., Executive MBA, has previously held Chief Geophysicist position, for 10 years, in a gold-platinum mining company extensively used in its mineral exploration programs borehole, ground and airborne geophysics. He has been associated with the airborne geophysics industry since 2005 (Aeroquest Limited and Geotech Ltd.) holding management positions as Regional General Manager, Data Interpretation Manager, Director of Geophysics and working on exploration projects for diverse commodities in regions over the world. He is an author and co-author of many publications dedicated to airborne EM. In 2019 he was awarded Barlow Medal for Best Geological Paper published in CIM publications (Canadian Institute of Mining, Metallurgy and Petroleum).

Services

Expert Geophysics Surveys Inc. specializes in airborne geophysical surveys with advanced electromagnetic systems. EGS offers surveying with Mobile MagnetoTellurics (**MobileMT**) and time domain electromagnetic system (**TargetEM**), the most advanced generation of airborne AFMAG technologies. The patent pending **MobileMT** technology utilizes naturally occurring electromagnetic fields in the frequency range of 25 Hz – 30 000 Hz. While the high-quality signal **TargetEM** technology induces eddy currents that generate secondary EM fields which can be measured in the range of 13 micro sec - 21701 micro sec. The **MobileMT** and **TargetEM** technologies are the product of extensive experience in developing equipment and signal/data processing algorithms for natural and induced electromagnetic field measurement, both technologies combine the latest advances in electronics, airborne system design, and sophisticated signal processing techniques.

Appendix II MobileMT Electromagnetic Technology



MobileMT (Mobile MagnetoTellurics) is a newly developed approach to electromagnetic data acquisition from synchronized a towed three component inductive magnetic sensor and grounded two orthogonal electric lines. The system is designed and implemented in order to overcome existing limitations of airborne techniques based on passive electromagnetic fields principles and, ultimately, for improving exploration efficiency.

MobileMT is a passive airborne electromagnetic technique that records magnetic (in the air) and electric (on the ground) fields generated by natural sources in the audio frequency range. The natural electromagnetic primary field sources for MobileMT are considered with frequencies ranging from 25 Hz to 30 kHz (ELF+VLF). The exploration system includes two pairs of grounded electric wire lines, one of them is for reference signal, and moving three-component inductive coil system softly suspended and with low-noise signal amplifiers for magnetic field measurements (dB/dt) in three orthogonal directions. A crucial element of the technology is the capability of aerial acquisition magnetotelluric data in four decades frequency band. Field data are acquired using stationary orthogonal pairs of electrical field sensors (grounded wire dipoles) and towed magnetic field detectors (three orthogonal induction coils).

In order to continue evolution of the airborne electromagnetic passive fields technology and in comparison with the last AFMAG development (Bob Lo, 2009) the current development is focused on:

- Expanding measured frequencies range into high end to complement deep exploration with near surface, shallow and medium depth of investigation;
- Increasing sensitivity and reducing system noise level to provide with data at low natural electromagnetic fields signal conditions especially in the range of the last hundred – first thousands Hz frequencies band where the field spectral density is lowest (dead-band);
- Providing ability to recover electrical properties differences between geological boundaries of any direction, including and between horizontal and vertical boundaries;
- Increasing spatial and frequency data resolution;
- Measuring of elements of admittance-type transfer functions of the magnetotelluric field.

Theory and Method

Some part of the thunderstorm energy is converted into electromagnetic fields that are propagated in the ionosphere-Earth interspace. These electromagnetic fields and the currents induced by these fields in the subsurface are used in audiomagnetetotelluric prospecting to measure the electrical resistivity of geological environment.

Measuring telluric currents induced by the natural electromagnetic fields in the subsurface on the ground synchronised with measuring the magnetic components of the natural audio frequency electromagnetic fields in the air and mutual processing both airborne and ground data (Figure 1) is a way to improve the quality and increase informative of the measured airborne data. In practice the reference fields may be measured by inductive coils or grounded electric lines (Labson et al., 1985). To obtain accurate signal of the natural field spectrum and eliminate noise spectra of sensors we use electrical field measurements at the base station. One of the reasons of choosing electrical components for reference is capacity to control the natural signal strength in the wire lines. Each electrical field component on the base station is registered independently from two sensors, signal and reference, which is utilized to eliminate the data bias distortions (Labson et al., 1985). This technical solution is critically helpful in periods of weak natural field signals in some frequency bands.

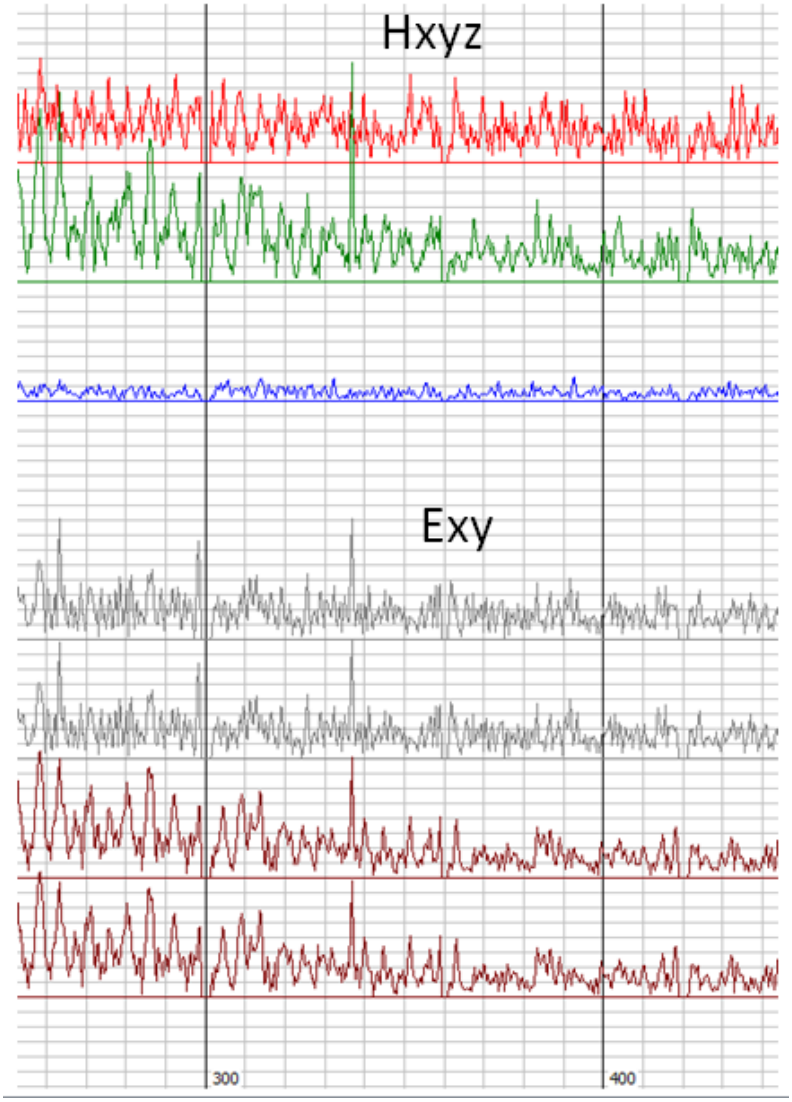


Figure 1. A section of time series of Exy and Hxyz data

Exploiting signals of two horizontal electric components along with three magnetic components we can process them with the magnetotellurics response functions based on linear relations between components of the electric and magnetic fields. In general, processing of the field data is based on the

Larsen and Chave robust remote-reference method (Chave et al., 1987; Larsen, 1989). The data processing program merges the stationary measured electrical two horizontal components and the moving orientation irrelevant receiver of three magnetic field components into one file. The program applies FFT technique to the recordings and calculates the matrixes of the relations between the electric and magnetic signals (six admittances) on the different time bases and in different frequency bands. In the result of modular computation of the matrixes determinants, as rotation invariant parameters, we calculate apparent conductivity in mS/m as a parameter of EM mapping. The rotation invariant parameters are free from the receiver motion distortions. The admittances (***Y***) are represented as the electric field horizontal vectors projection into the space of the magnetic field three components. In other words, the combined system measures combination of tensor and scalar (rotational invariant) components as the transfer function of a total magnetic field, through the three orthogonal directions measurements of an airborne receiver, to the two orthogonal horizontal directions of electric field measured at a ground base location. Generalizing the Weiss-Parkinson relationship (Berdichevsky and Zhdanov, 1984), such as that measured three orthogonal magnetic field components (***H***xyz) are linearly related to the horizontal electric fields measured on the ground (***E***xy, reference), with adoption it to the admittances domain (***Y***):

$$\begin{bmatrix} Hx \\ Hy \\ Hz \end{bmatrix} = \begin{bmatrix} Yxx & Yxy \\ Yyx & Yyy \\ Yzx & Yzy \end{bmatrix} \begin{bmatrix} Ex \\ Ey \end{bmatrix} \quad (1)$$

Solutions of the equations are obtained by averaging over a number of closely spaced frequencies (see table below).

An example of frequency windows used for harmonics averaging. Base 15 Hz, Gates ratio 2.

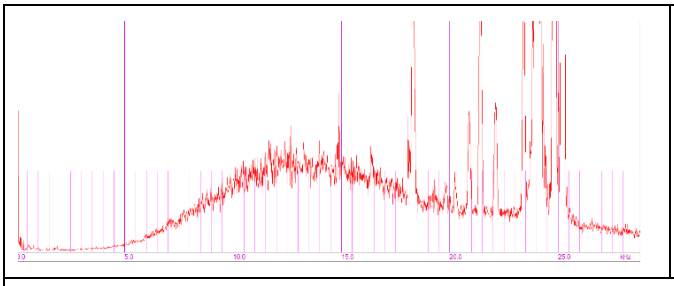
N	Window, Hz		
	start	end	mid
1	15	30	23
2	30	68	49
3	68	135	101
4	135	270	203
5	270	540	405
6	540	1080	810
7	1080	2160	1620
8	2160	4320	3240
9	4320	8640	6480
10	8640	17280	12960
11	17280	28800	23040

The windowing way is flexible and can be optimized depending on signals, cultural noise, and an exploration task.

H (magnetic) and ***E*** (electric) components time series data, fully synchronized, digitized, and recorded at 73,728 Hz frequency, is converted from time to frequency domain using FFT technique. The complex data spectrums (field examples in 2 and 3) is expressed in apparent conductivity (σ) equivalent to its real part:

$$\boldsymbol{\sigma = \mu\omega|Y^2|} \quad (2)$$

where $\boldsymbol{Y}$ is the determinant of the corresponding matrix in (1); $\boldsymbol{Y}^2 = \text{im}(\boldsymbol{Y}^2)/\text{re}(\boldsymbol{Y}^2)$; μ is the magnetic permeability of free air and ω is the angular frequency.



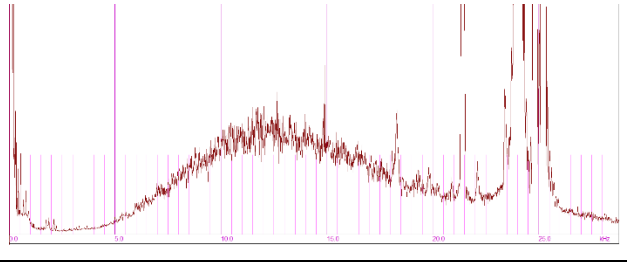
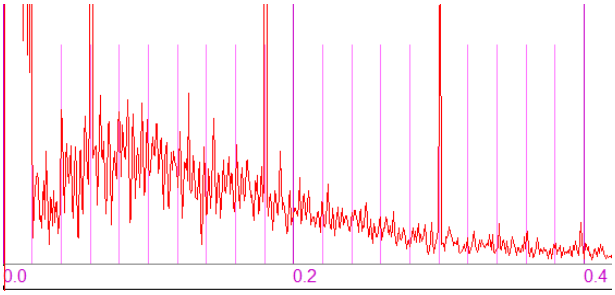


Figure 2 Airborne magnetic X-coil spectrum up to 30,000 Hz range (left) with the corresponding electric X-line 1 spectrum (right)



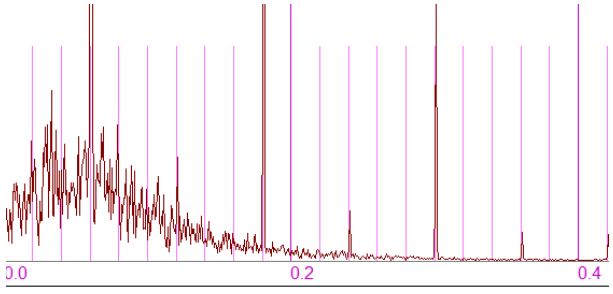


Figure 3 Airborne magnetic X-coil spectrum up to 400 Hz range (left) with the corresponding electric X-line 1 spectrum (right)

References

Berdichevsky, M.N., and M.S. Zhdanov (1984), Advansed theory of deep geomagnetic sounding: Elseiver.

Chave, A. D., Thomson, D. J., and Ander, M. E. (1987), On the Robust Estimation of Power Spectra, Coherences, and Transfer Functions: Journal of Geophysical Research, **92**, 633-648.

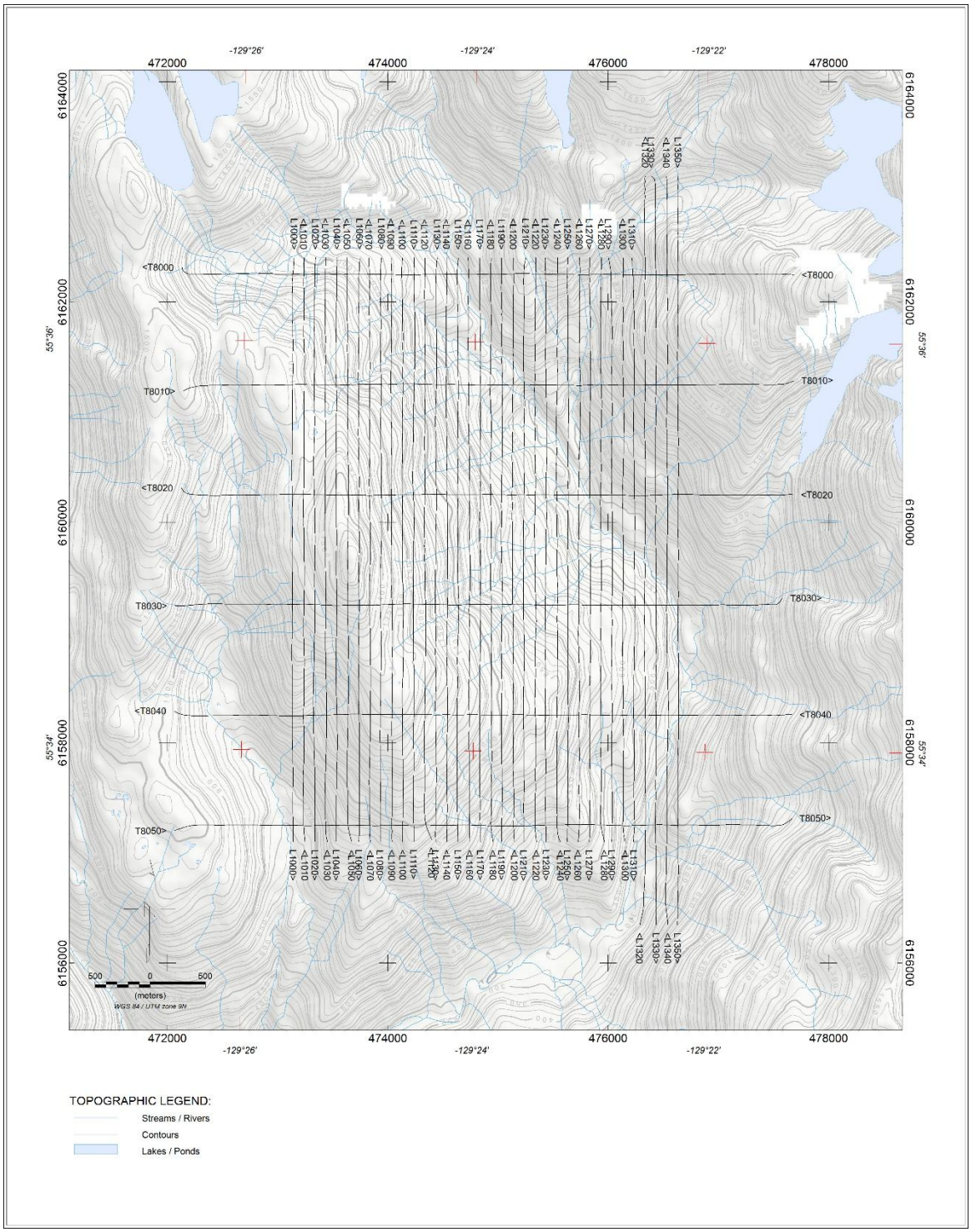
Labson, V.F., A.Becker, H.F.Morrison, and U.Conti (1985), Geophysical exploration with audio frequency natural magnetic fields: Geophysics, **50**, 656-664.

Larsen, J. C. (1989), Transfer functions: smooth robust estimates by least-squares and remote reference methods: Geophysical Journal International, **99**, 645-663.

Lo, B., J. Legault, P.Kuzmin (2009), Z-TEM (airborne AFMAG) tests over unconformity uranium deposits. Extended Abstract 20th International Geophysical Conference and Exhibition, Adelaide, South Australia.

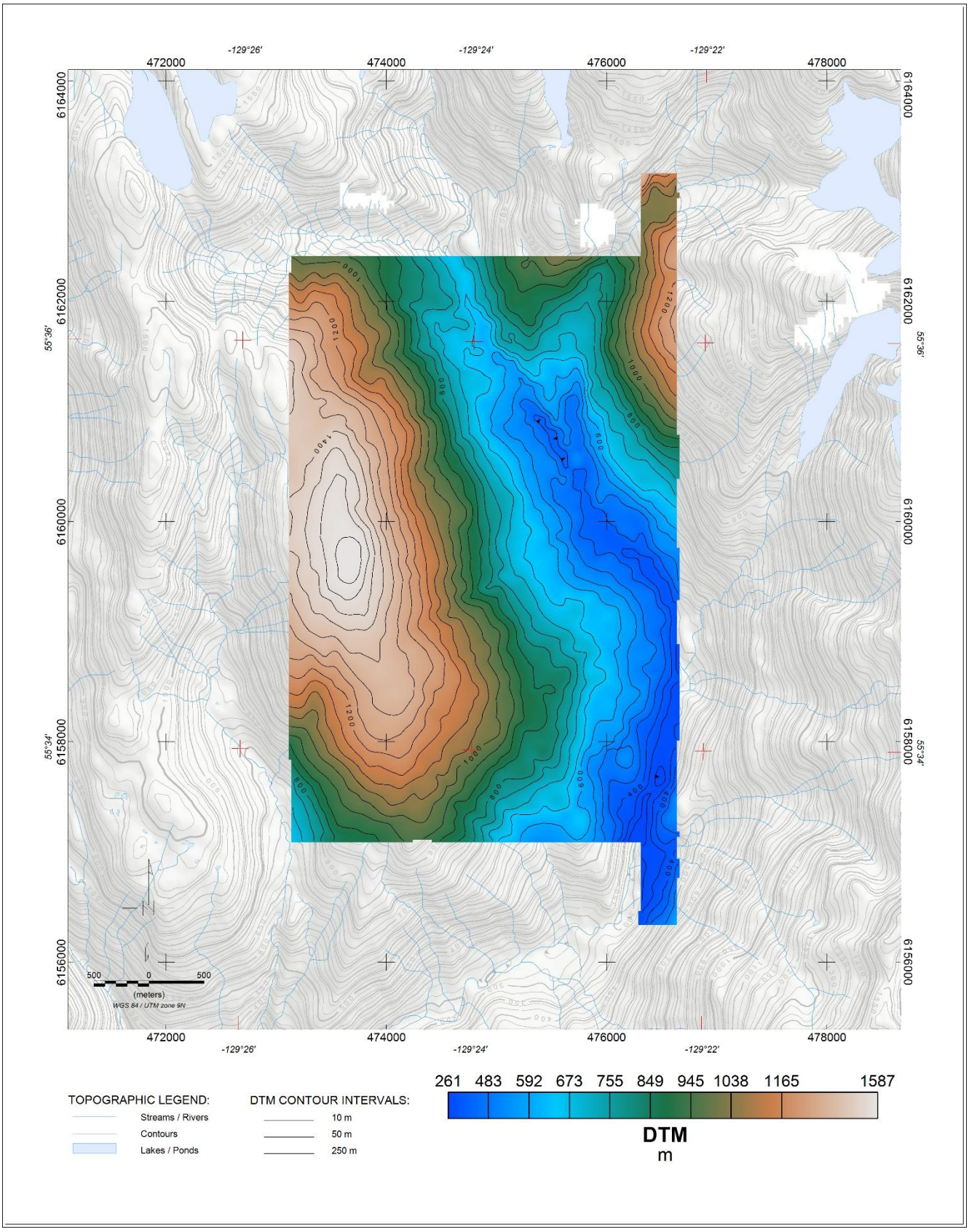
Appendix III MobileMT Maps Images [1]

Ajax Block

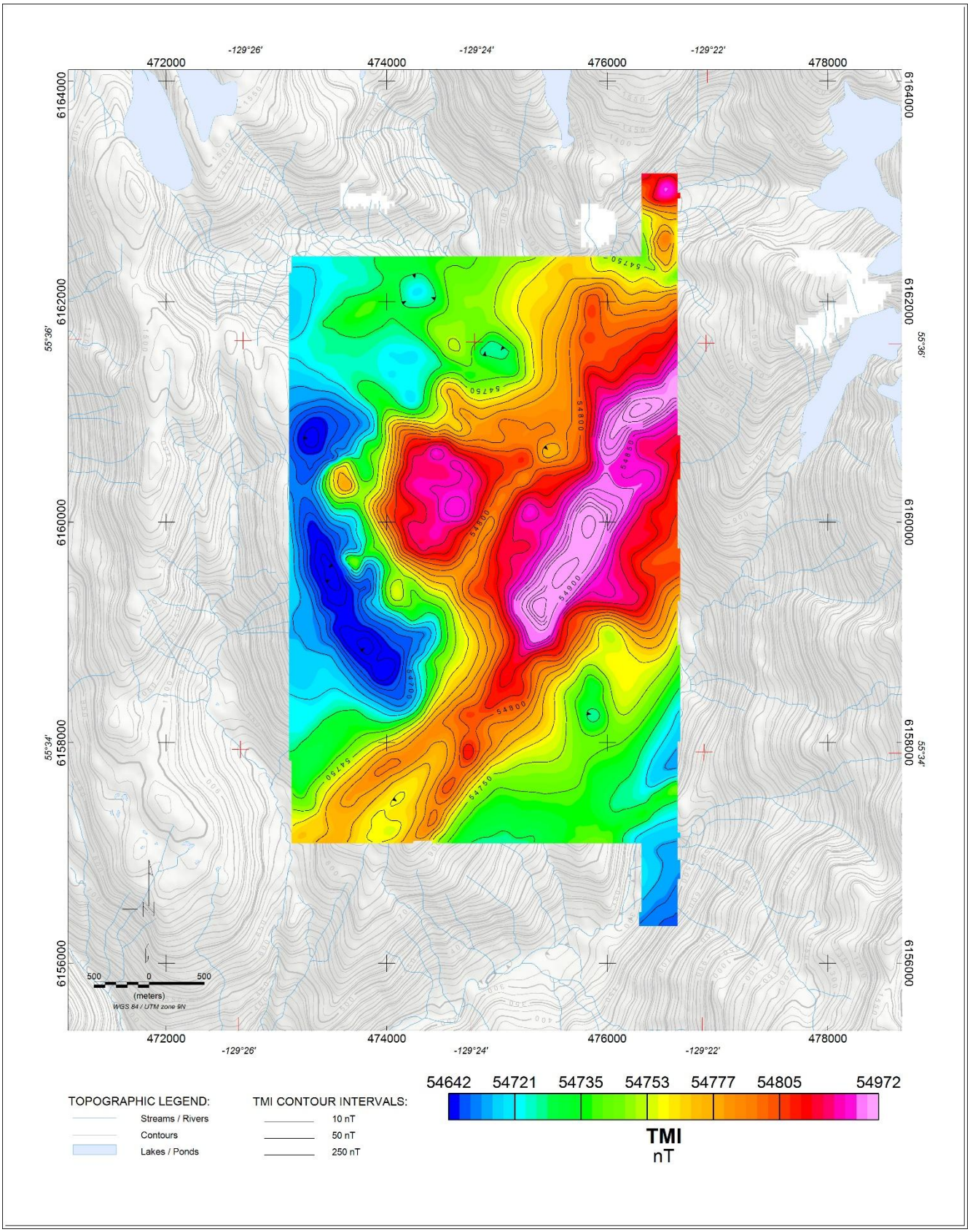


Line Path

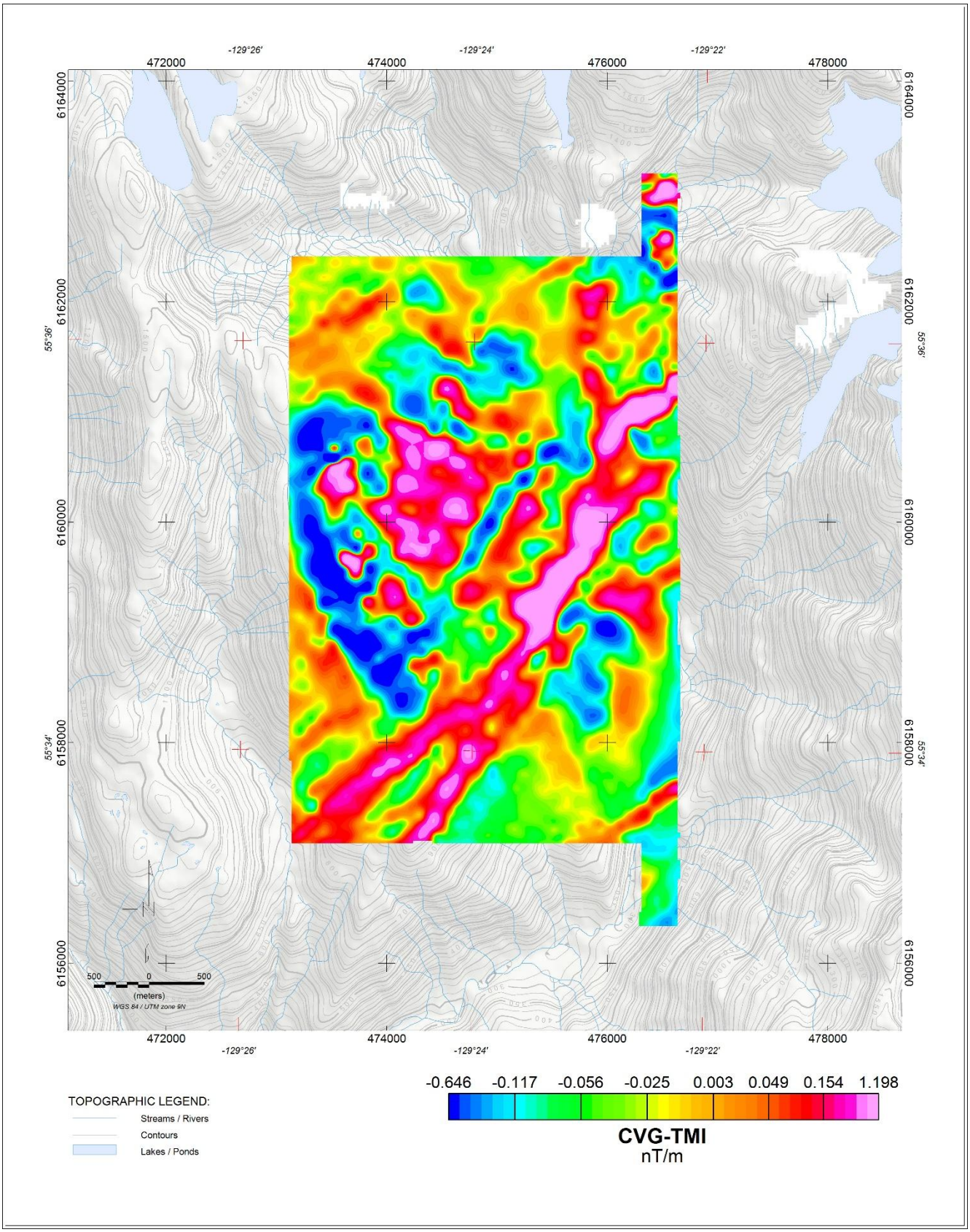
[1] Only selected maps are presented in the Appendix. A full set of maps is following the report in geosoft and pdf formats.



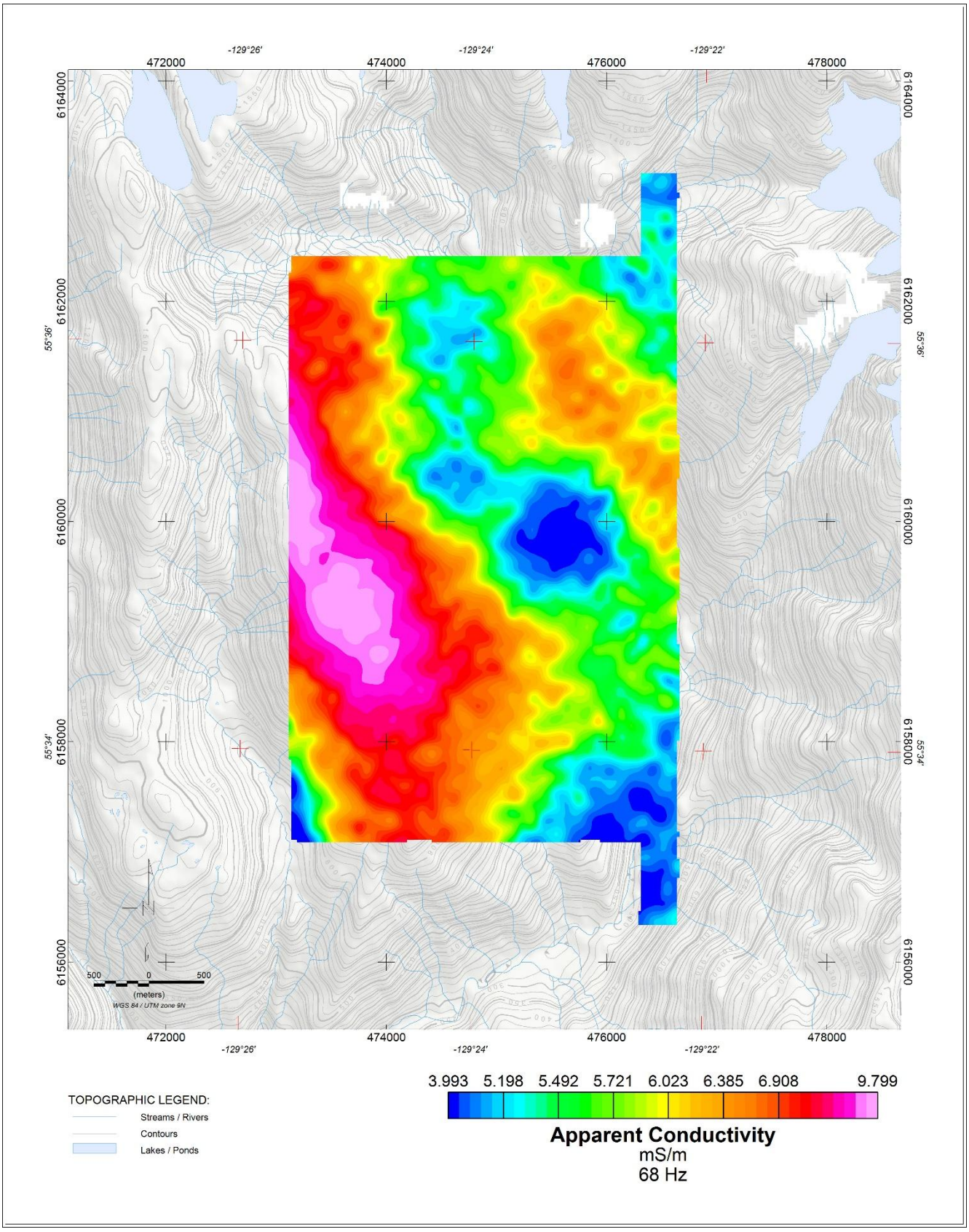
Digital Terrain Model (DTM)



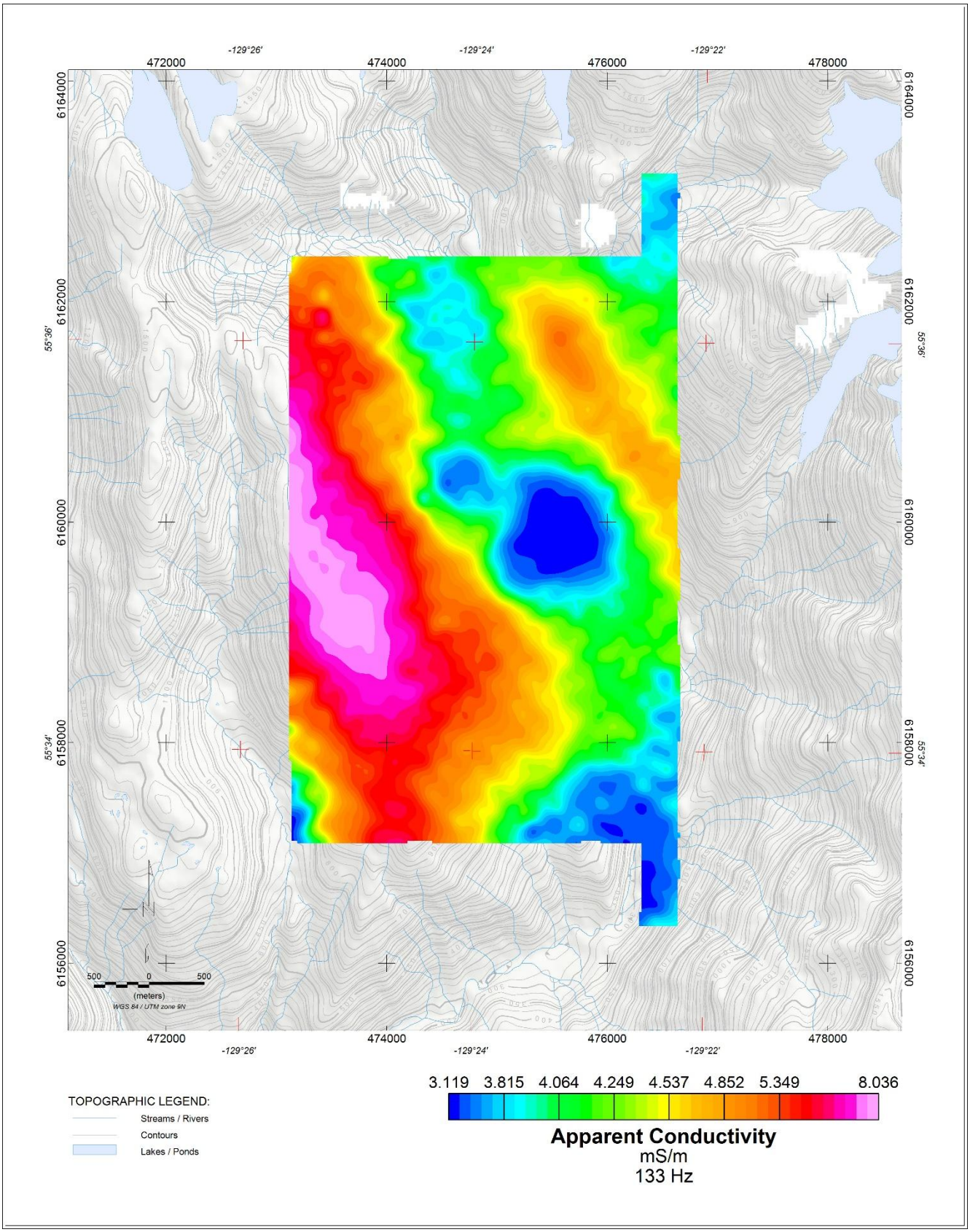
Total Magnetic Intensity Map (TMI)



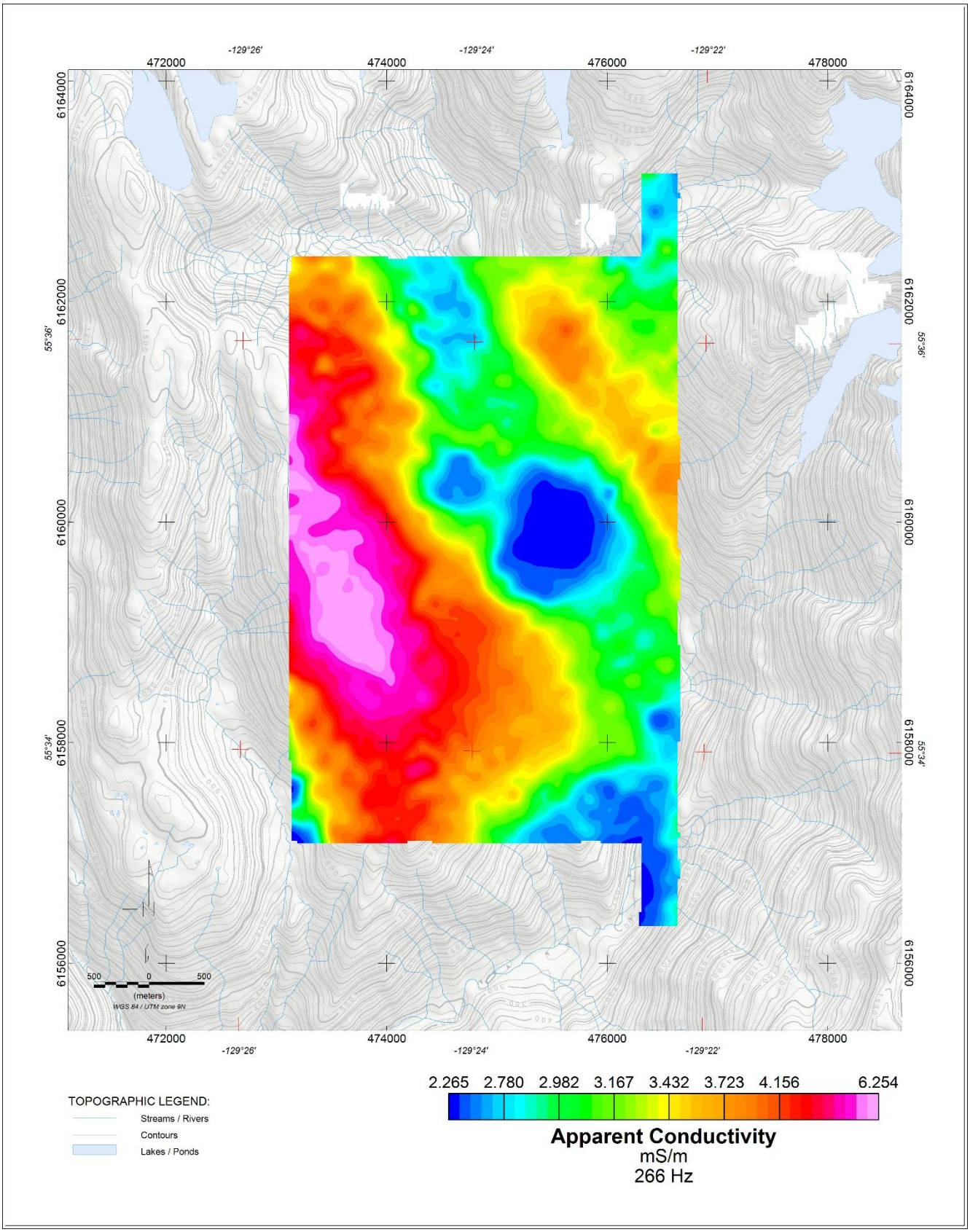
Calculated Vertical Derivative Map of magnetic field (CVG-TMI)



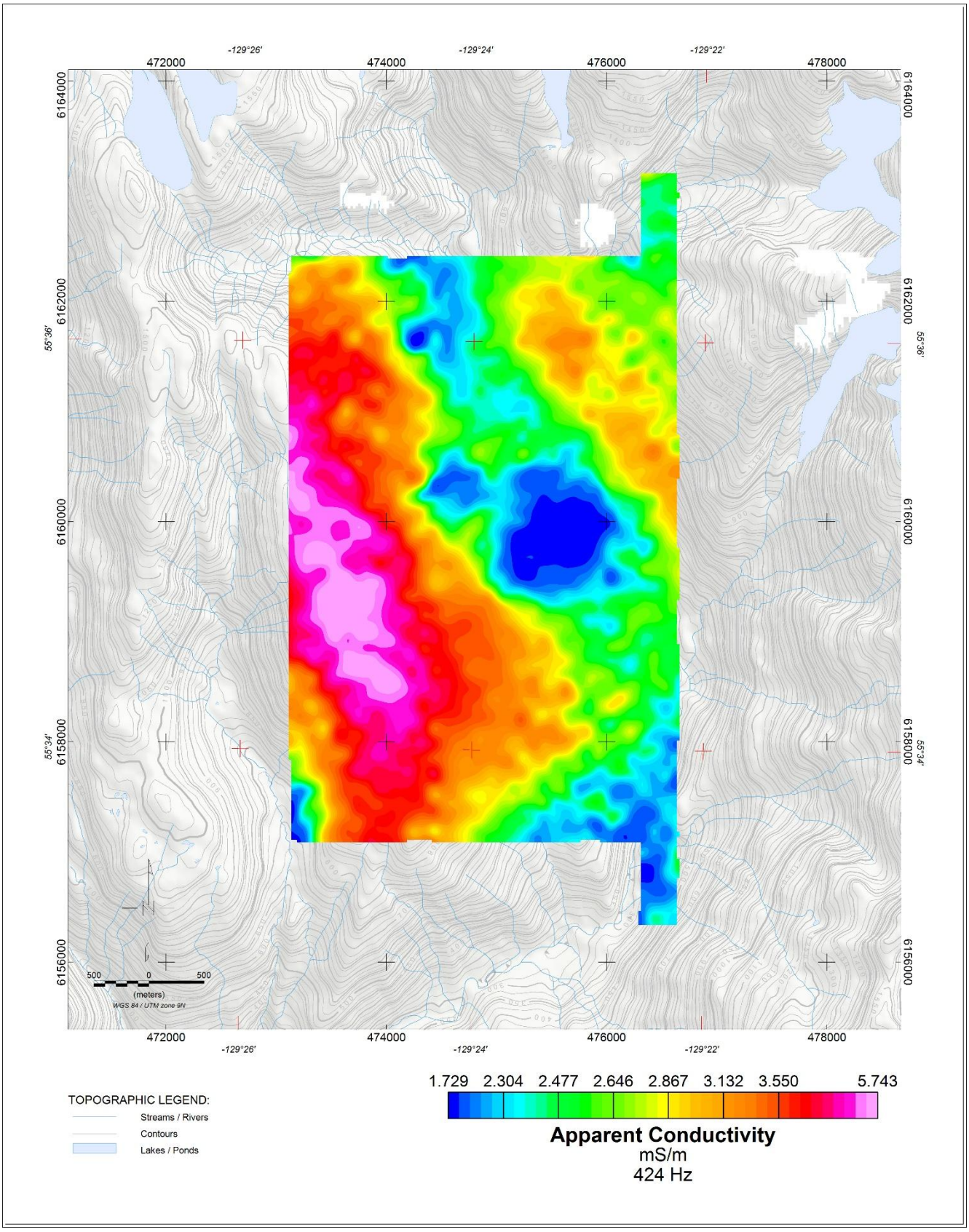
Apparent conductivity (68 Hz)



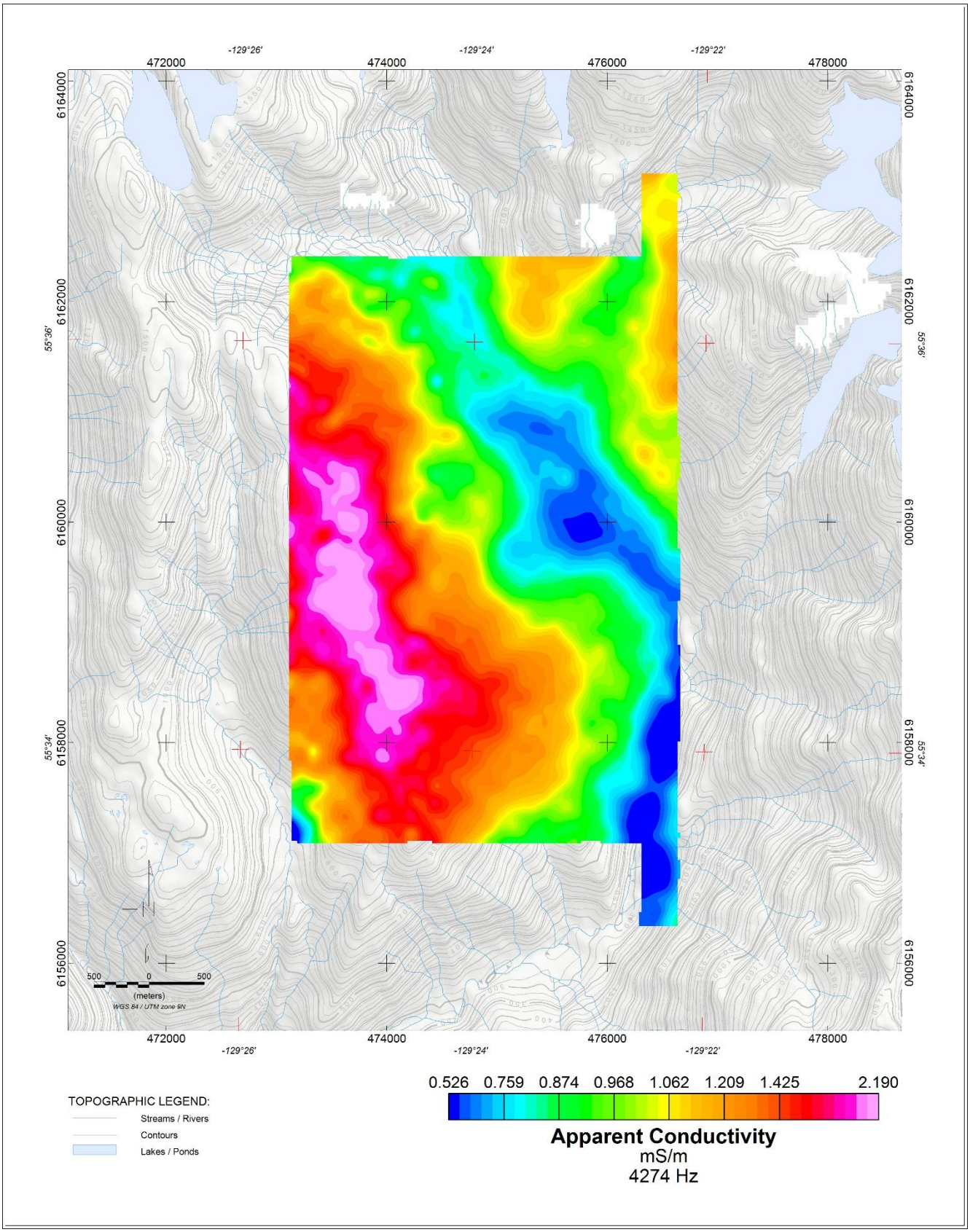
Apparent conductivity (133 Hz)



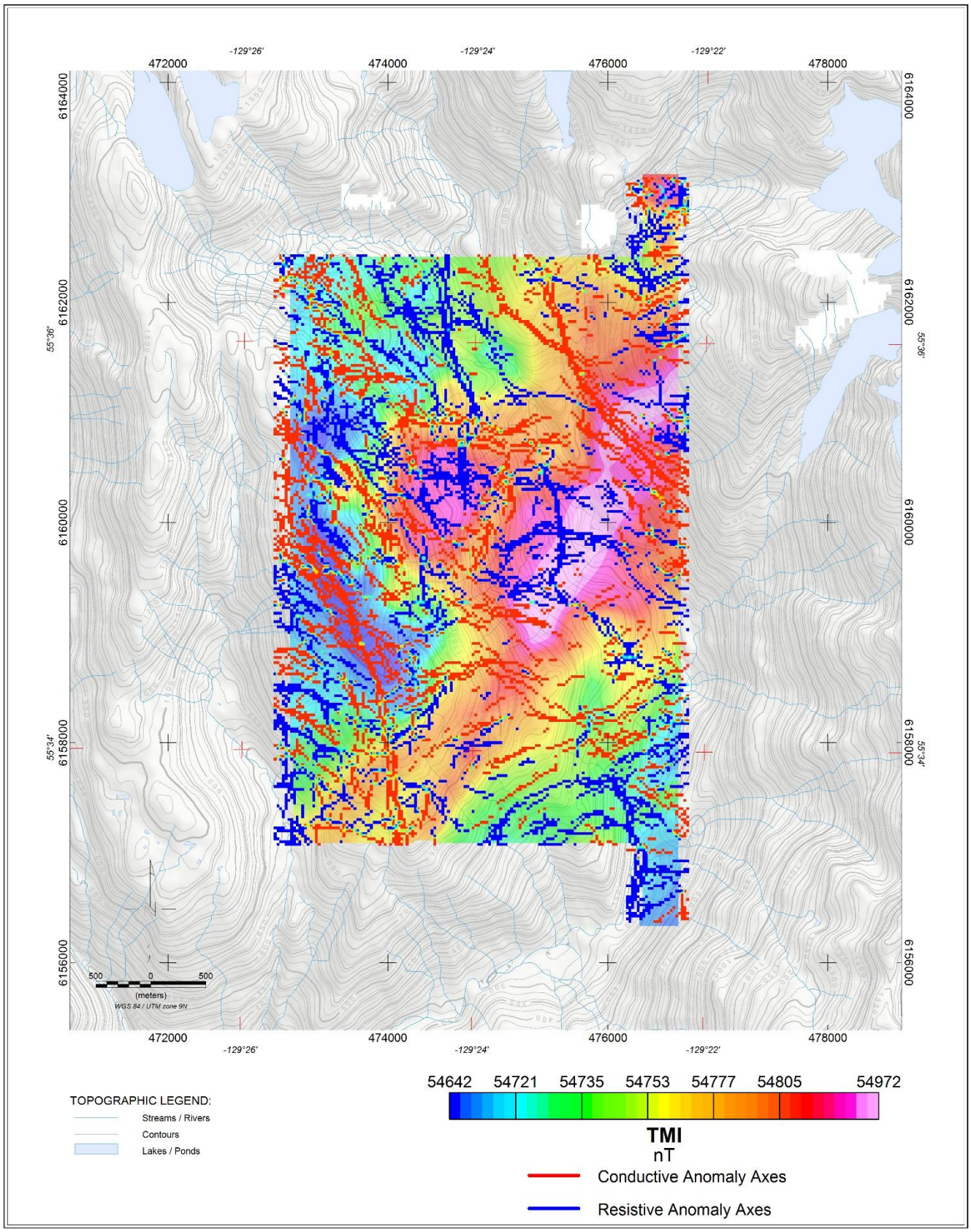
Apparent conductivity (266 Hz)



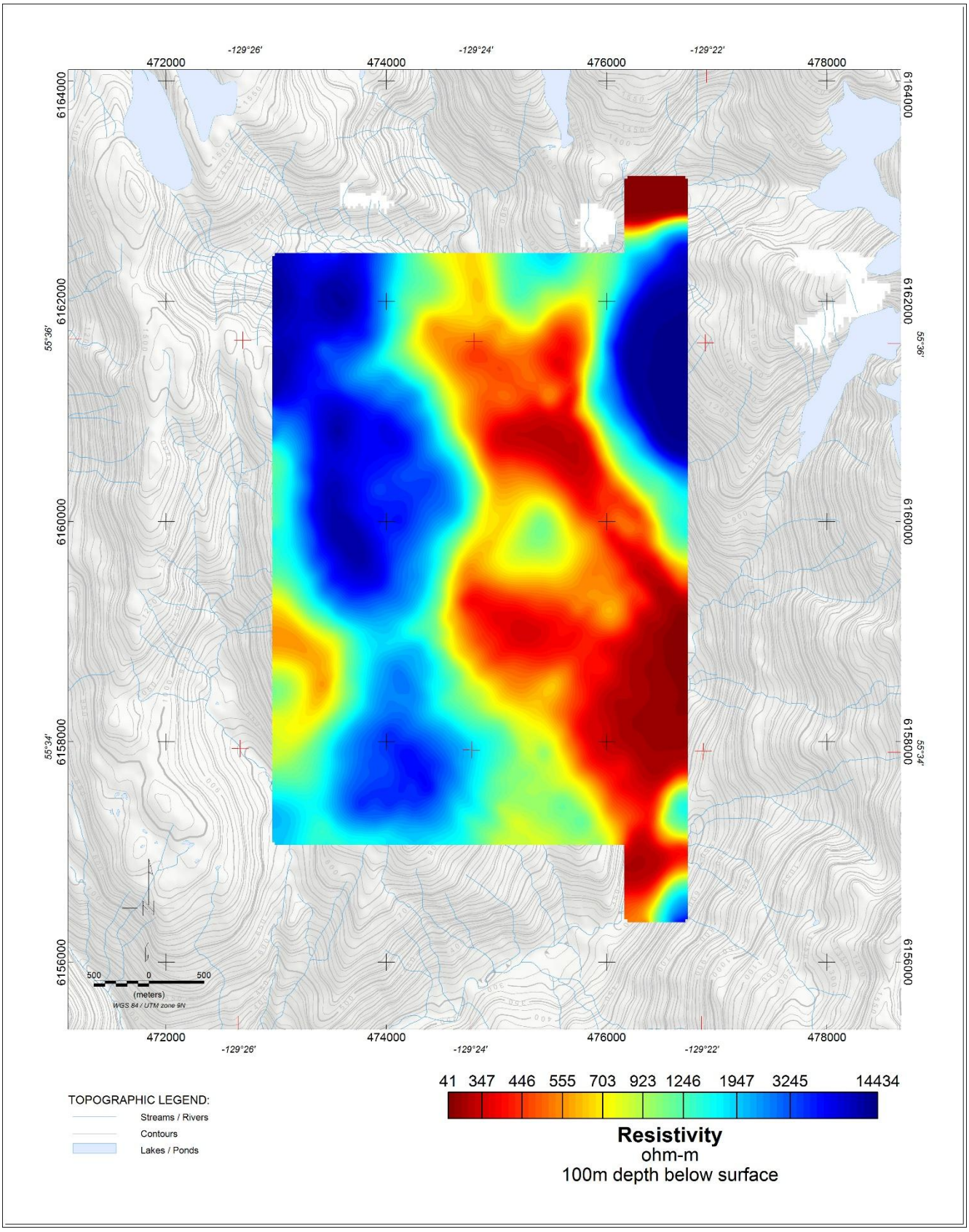
Apparent conductivity (424 Hz)



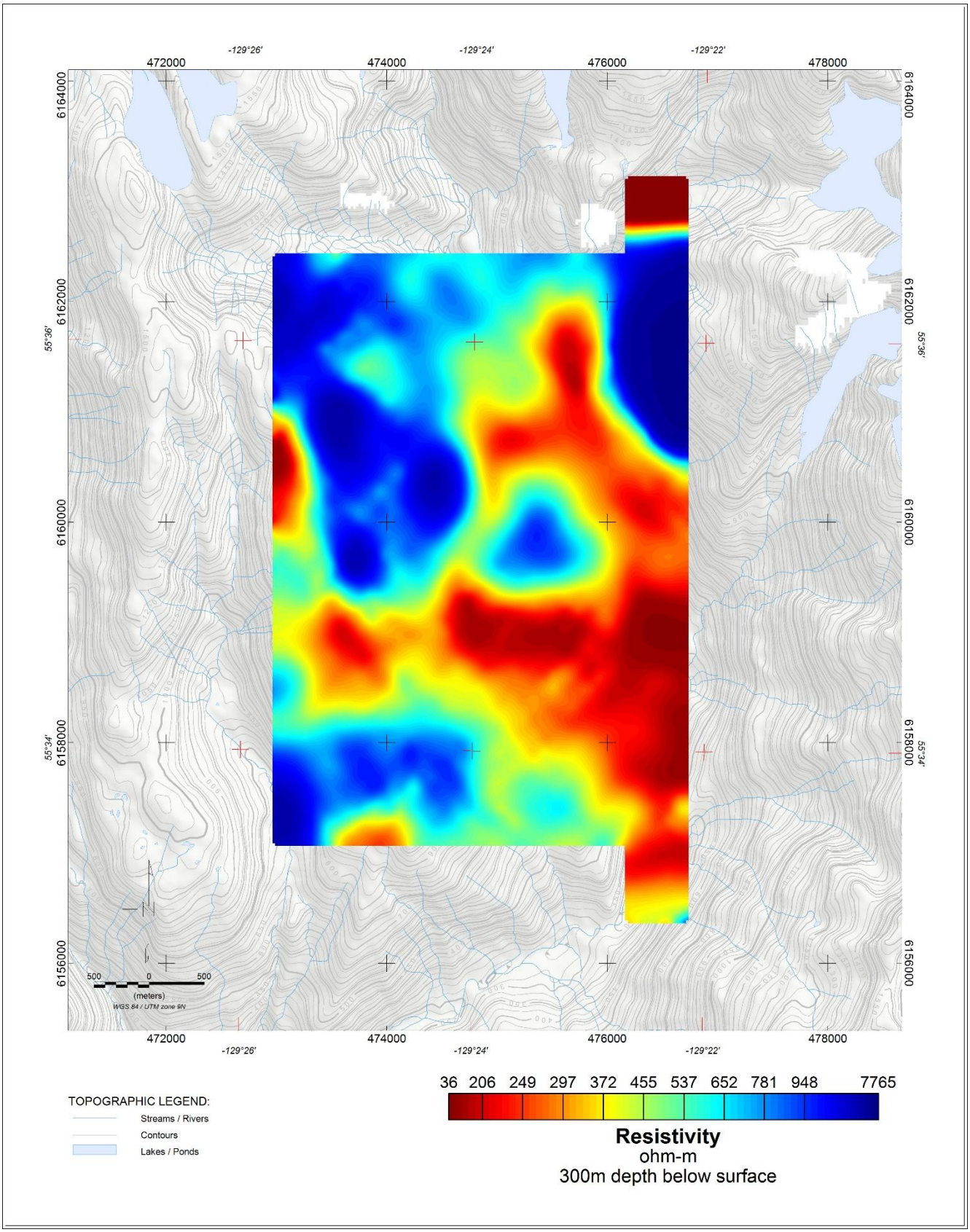
Apparent conductivity (4274 Hz)



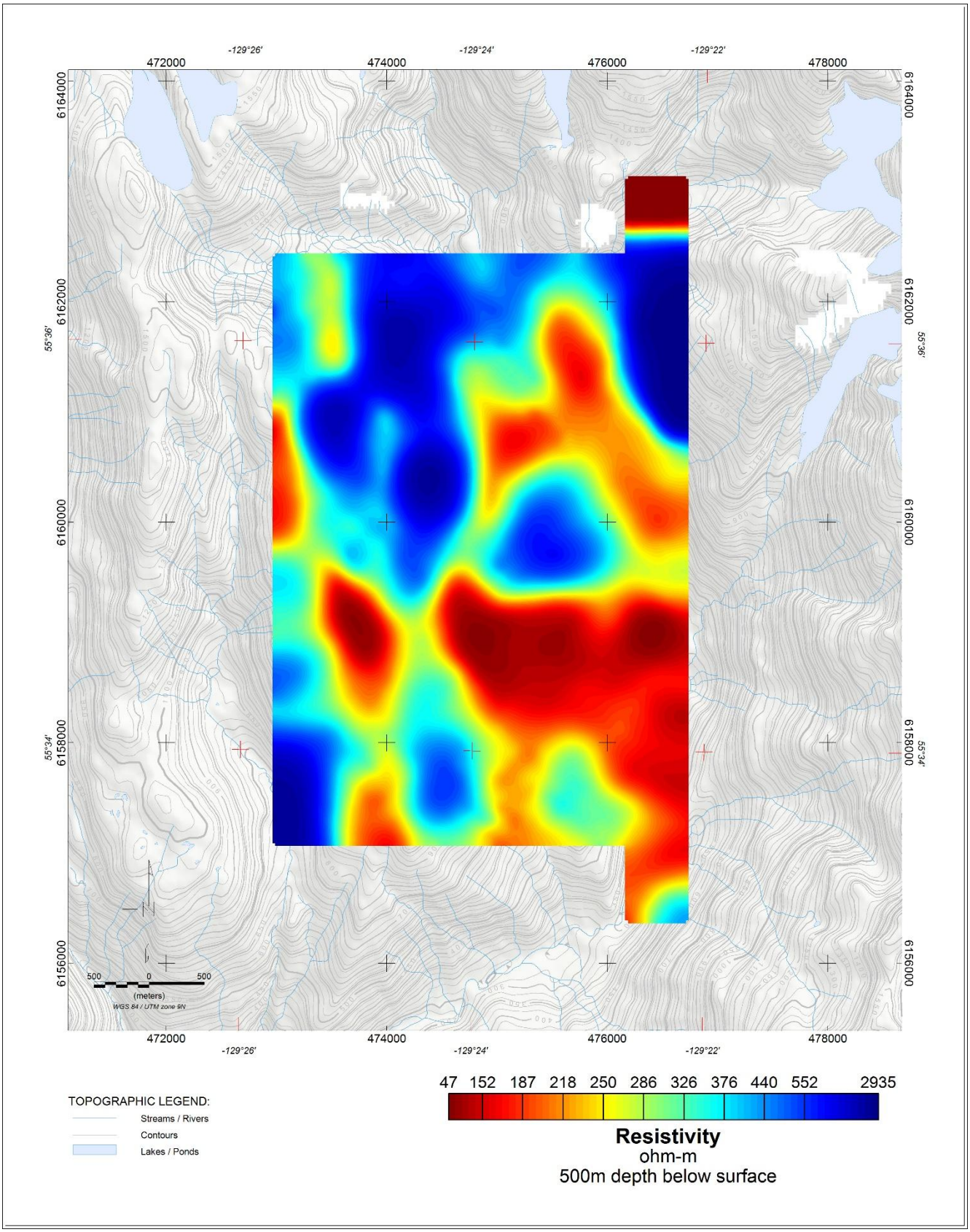
Axes of apparent conductivity anomalies in the frequency range 106-212 Hz over TMI color grid



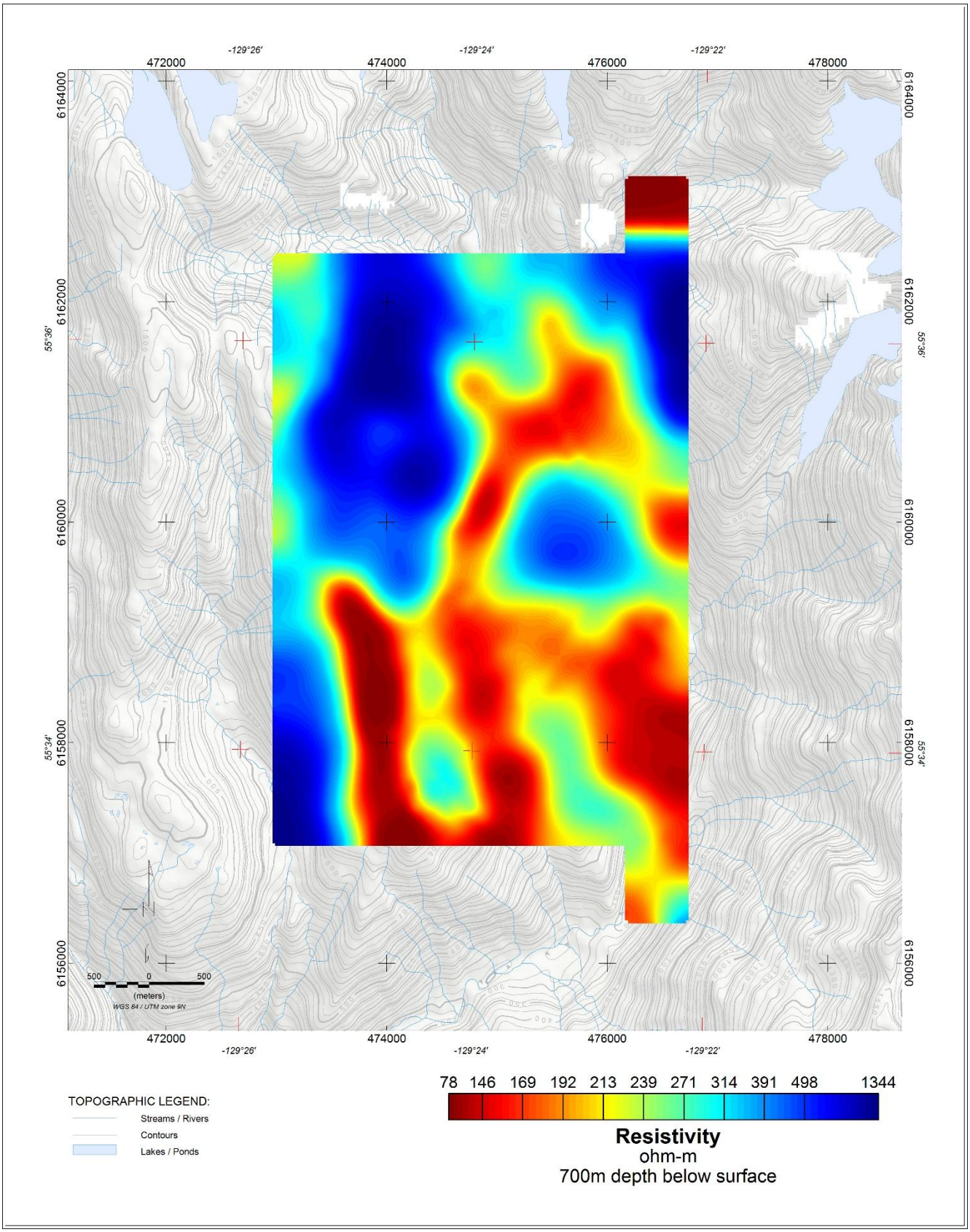
Resistivity at 100m depth below surface (determined through inversions)



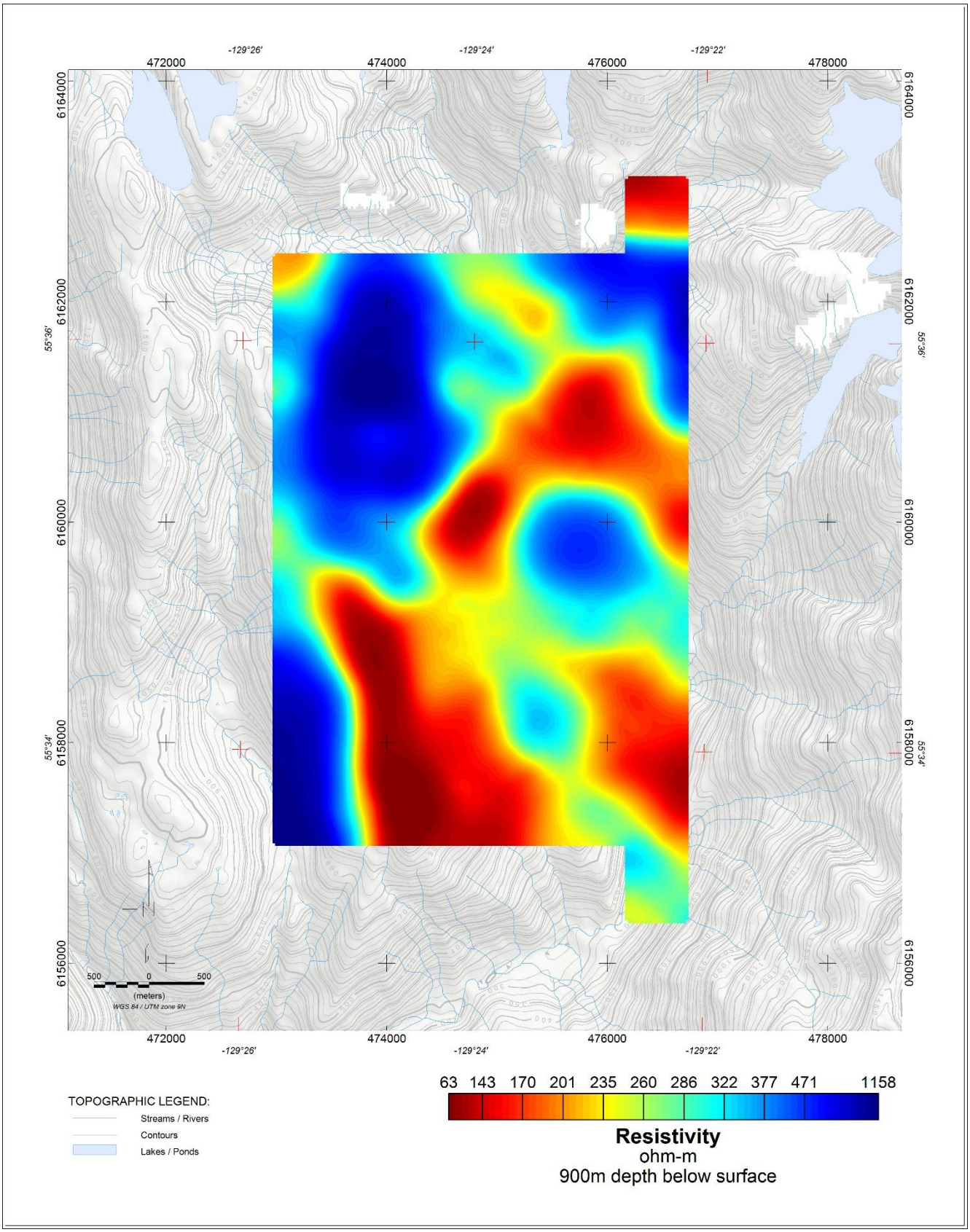
Resistivity Depth Slice at 300 m



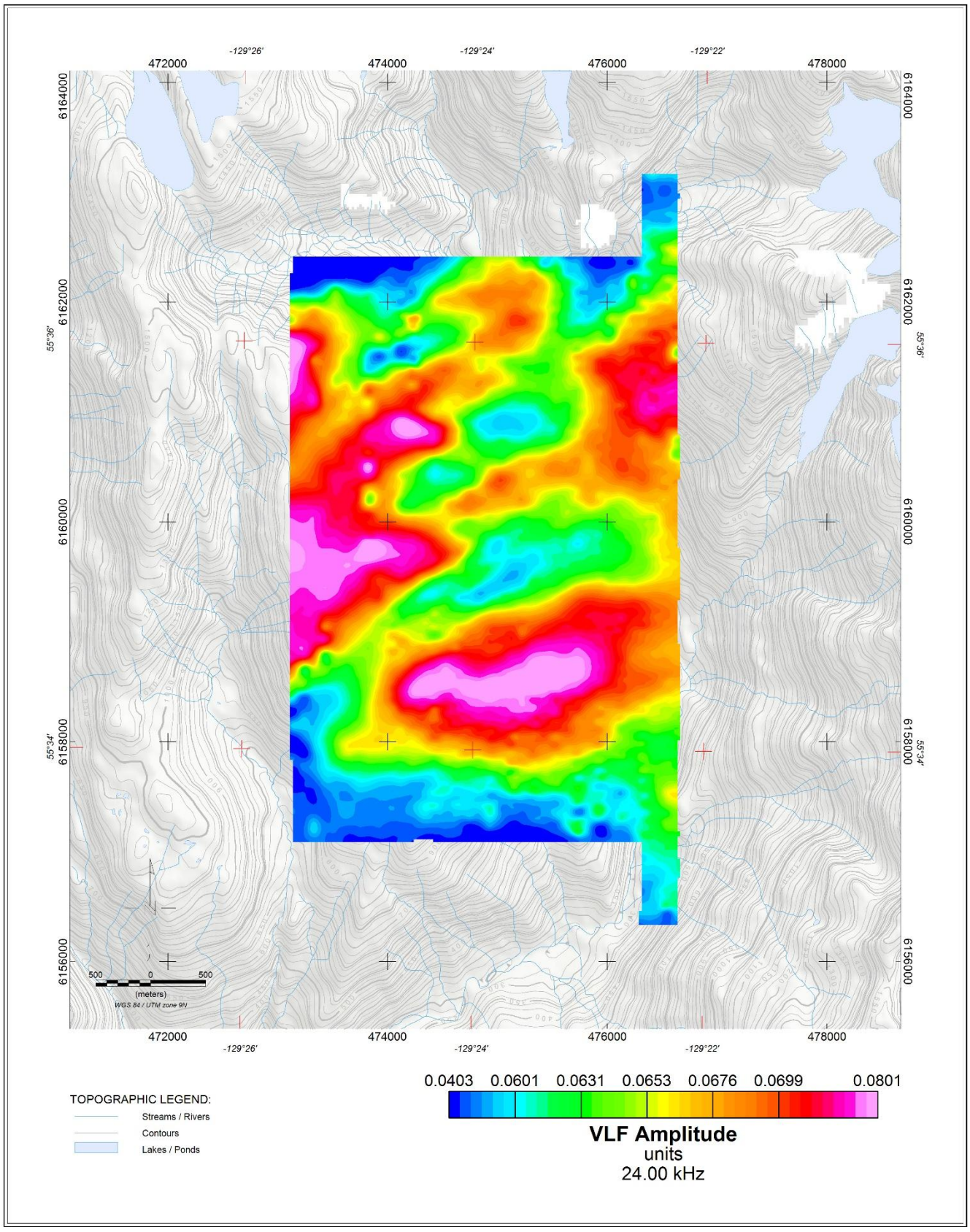
Resistivity Depth Slice at 500 m



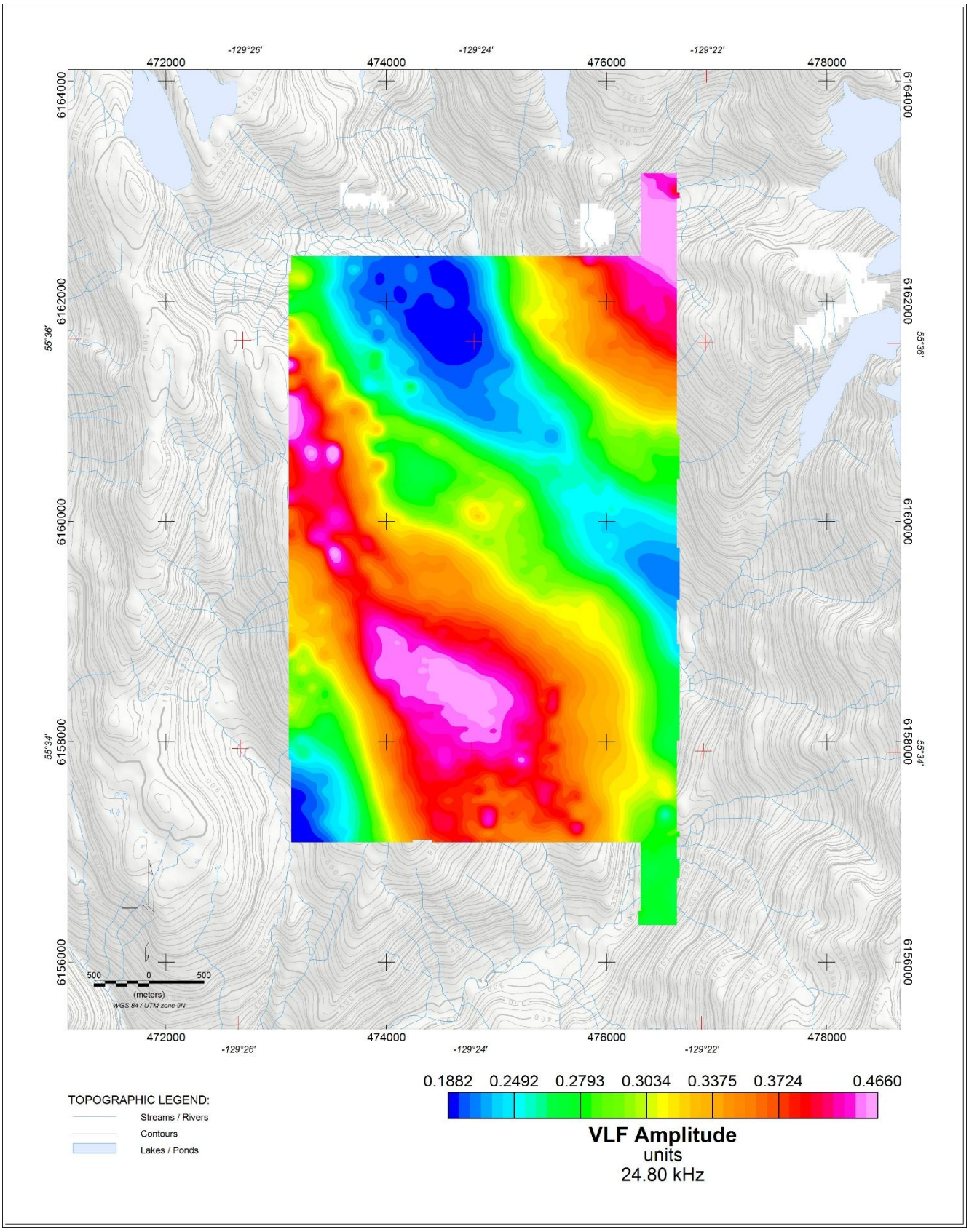
Resistivity Depth Slice at 700 m



Resistivity Depth Slice at 900 m



VLF Amplitude Map (24.00 kHz)



VLF Amplitude Map (24.80 kHz)